Kamada H., Nakagawa S., Tsunoda S., *Biol. Pharm. Bull.*, **29**, 1325–1330 (2006).

5) Nahta R., Esteva F. J., *Cancer Chemother. Pharmacol.*, **53**, 186–190 (2004).

6) Nahta R., Yu D., Hung M. C., Hortobagyi G. N., Esteva F. J., *Nat. Clin. Pract. Oncol.*, **3**, 269–280 (2006).

7) Amar S., Moreno-Aspitia A., Perez E. A., *Breast Cancer Res. Treat.*, **109**, 1–7 (2008).

8) Vannucchi S., Chiantore M. V., Fiorucci G., Percario Z. A., Leone S., Affabris E., Romeo G., *Oncogene*, **24**, 2536–2546 (2005).

9) Plummer R., Attard G., Pacey S., Li L., Razak A., Perrett R., Barrett M., Judson I., Kaye S., Fox N. L., Halpern W., Corey A., Calvert H., de Bono J., *Clin. Cancer Res.*, **13**, 6187–6194 (2007).

10) Tolcher A. W., Mita M., Meropol N. J., von Mehren M., Patnaik A., Padavic K., Hill M., Mays T., McCoy T., Fox N. L., Halpern W., Corey A., Cohen R. B., *J. Clin. Oncol.*, **25**, 1390–1395 (2007).

11) Fukunaga Y., Bandoh S., Fujita J., Yang Y., Ueda Y., Hojo S., Dohmoto K., Tojo Y., Takahara J., Ishida T., *Lung Cancer*, **38**, 31–38 (2002).

12) Wolff J. M., Borchers H., Brehmer B. Jr., Brauers A., Jakse G., *Urol. Int.*, **60**, 152–155 (1998).

13) Ditzel H. J., Strik M. C. M., Larsen M. K., Willis A. C., Waseem A., Kejling K, Jensenius J. C., *J. Biol. Chem.*, **277**, 21712–21722 (2002).

Science Signaling

Online issue 16 November 2010

BIOCHEMISTRY

Solution of the Structure of the TNF-TNFR2 Complex

Yohei Mukai,[1,2*] Teruya Nakamura,[3] Mai Yoshikawa,[1,2] Yasuo Yoshioka,[1,2,4] Shin-ichi Tsunoda,[1,4,5*] Shinsaku Nakagawa,[2] Yuriko Yamagata,[3] Yasuo Tsutsumi[1,4,6*]

(Published 16 November 2010; Volume 3 Issue 148 ra83)

Tumor necrosis factor (TNF) is an inflammatory cytokine that has important roles in various immune responses, which are mediated through its two receptors, TNF receptor 1 (TNFR1) and TNFR2. Antibody-based therapy against TNF is used clinically to treat several chronic autoimmune diseases; however, such treatment sometimes results in serious side effects, which are thought to be caused by the blocking of signals from both TNFRs. Therefore, knowledge of the structural basis for the recognition of TNF by each receptor would be invaluable in designing TNFR-selective drugs. Here, we solved the 3.0 angstrom resolution structure of the TNF-TNFR2 complex, which provided insight into the molecular recognition of TNF by TNFR2. Comparison to the known TNFR1 structure highlighted several differences between the ligand-binding interfaces of the two receptors. Additionally, we also demonstrated that TNF-TNFR2 formed aggregates on the surface of cells, which may be required for signal initiation. These results may contribute to the design of therapeutics for autoimmune diseases.

INTRODUCTION

Tumor necrosis factor (TNF) is an immunity-modulating cytokine that is required for defense against infectious diseases and carcinogenesis (*1*). Excess amounts of TNF, however, cause various autoimmune diseases, such as rheumatoid arthritis (RA), Crohn's disease, and ulcerative colitis (*2–4*). TNF activates signals through its two receptors [the type I TNF receptor (TNFR1) and TNFR2], and these molecules are well-known targets in therapies against autoimmune diseases (*1*, *5*). Currently, TNF neutralization therapies through the use of a soluble TNFR2-Fc chimera (etanercept), a mouse-human chimera monoclonal antibody against TNF (infliximab), or a fully humanized monoclonal antibody against TNF (adalimumab) have proven to be effective treatments for RA (*6*, *7*). Unfortunately, however, a block of TNF-mediated host defense often increases the risk of bacterial or viral infection (*8*, *9*) or of the development of lymphoma (*10*). Thus, a thorough understanding of the function of the TNF-TNFR complex is important for the design of optimal therapies against the various TNF-related autoimmune diseases.

TNFR1 and TNFR2 activate distinct cell signaling pathways. TNFR1 is ubiquitously expressed, whereas TNFR2 is found mostly on certain populations of immune cells. In general, TNFR1 is largely associated with the apoptotic activity of TNF, whereas TNFR2 is involved in T cell survival (*11*). Thus, both proteins must be fully analyzed to better understand the function of TNF. Previous studies with animal models of diseases such as arthritis and hepatitis demonstrated the predominant role of TNFR1 in the pathogenesis and exacerbation of inflammation (*12*, *13*). Nonetheless, TNFR2 is crucial for antigen-stimulated activation and proliferation of T cells (*14–16*), which is essential for cell-mediated immunity to pathogens. In addition, transmembrane TNF (tmTNF), the prime activating ligand of TNFR2 (*17*), is sufficient to control infection by *Mycobacterium tuberculosis* (*18*, *19*), indicating the importance of TNFR2 in this type of bacterial infection. Other reports showed that TNFR2 is important in the function of regulatory T cells (*20*), suggesting a role for tmTNF-TNFR2 signaling in anti-inflammatory effects. On the basis of these studies, the specific blocking of TNFR1 signaling appears to be a promising approach to minimize the side effects that are associated with "anti-TNF" therapy (*5*, *11*, *21*, *22*). Thus, it is highly desirable to establish a structural basis for the differences between TNFR1 and TNFR2.

One structural characteristic shared by most members of the TNFR superfamily is that they contain from about two to four cysteine-rich domains (CRDs) (*5*). The first structure of a TNFR superfamily member to be determined was the crystal structure of the lymphotoxin-α (LT-α)–TNFR1 complex (*23*). The authors of that study suggested that the protein fold is characterized by multiple disulfide linkages in the CRD and that these bonds are important in stabilizing the structure of the TNFR. Moreover, a trimer of LT-α binds to three TNFR1 monomers through CRD2 and CRD3 in TNFR1, suggesting that trimerization of TNFRs is directly related to their signaling. The structural similarity between TNF and LT-α suggests that TNF should be able to form a complex with TNFR1 that resembles that of LT-α–TNFR1 (*23–25*). More recently, the structures of complexes of other TNF-TNFR superfamily proteins have been solved, including TNF-related apoptosis-inducing ligand (TRAIL)–death receptor 5 (DR5) (*26–28*) and CD134 antigen (OX40) ligand (OX40L)–OX40 (*29*). These reports suggest that the structural features that were described for the LT-α–TNFR1 complex are common to other TNF-TNFR superfamily members. Moreover, a study revealed the crystal structure of TNF in a complex with a viral TNF inhibitor (poxvirus 2L protein) (*30*) that is important for viral escape from TNF-mediated immunity (*31*). Therefore, determination of the structure of TNFR2 and of its role in immunity against pathogens would be useful in understanding the details of basic TNF functions.

[1]Laboratory of Biopharmaceutical Research, National Institute of Biomedical Innovation, Osaka 567-0085, Japan. [2]Department of Biotechnology and Therapeutics, Graduate School of Pharmaceutical Sciences, Osaka University, Osaka 565-0871, Japan. [3]Graduate School of Pharmaceutical Sciences, Kumamoto University, Kumamoto 862-0973, Japan. [4]Center for Advanced Medical Engineering and Informatics, Osaka University, 1-6 Yamadaoka, Suita, Osaka 565-0871, Japan. [5]Department of Biomedical Innovation, Graduate School of Pharmaceutical Sciences, Osaka University, Osaka 565-0871, Japan. [6]Department of Toxicology and Safety Science, Graduate School of Pharmaceutical Sciences, Osaka University, Osaka 565-0871, Japan.
*To whom correspondence should be addressed. E-mail: yohe@phs.osaka-u.ac.jp (Y.M.); tsunoda@nibio.go.jp (S.T.); ytsutsumi@phs.osaka-u.ac.jp (Y.T.).

Another important characteristic of the TNFR superfamily is that many of these proteins exist as preassembled oligomers on the cell surface [for example, Fas (Apo-1/CD95), TNFR1, and TNFR2] (*32*, *33*). This ligand-independent assembly of TNFR oligomers is mediated by the preligand assembly domain (PLAD), which resides within the N-terminal CRD (CRD1) of the TNFRs and is not directly involved in binding to ligand (*33*). PLAD-mediated, ligand-independent assembly has also been reported for TRAIL receptors and viral homologs of TNFR (*34*, *35*). Ligand-independent assembly of receptors was reported for other cytokine members, such as the interleukin-17 receptor (*36*), which indicates that this phenomenon is important for various immune responses. Indeed, the PLAD of TNFRs is critical for TNF-mediated responses (*33*), and soluble PLAD can effectively prevent TNFR signaling and potently inhibit inflammatory arthritis (*37*). These results suggest that PLAD-mediated receptor assembly is essential for TNFR signaling. However, in the crystal structures of other TNF-TNFR superfamily complexes, such as TNFR1, DR5, and OX40, individual PLADs are disassociated (*23*, *26*–*29*). This apparent contradiction regarding PLAD-mediated receptor assembly must be resolved to understand the molecular basis for TNFR-mediated signal initiation. We reasoned that the behavior of the TNF-TNFR complex on the surface of live cells needed to be investigated to understand the molecular basis of the ligand-receptor interactions.

Here, we determined the first crystal structure of the TNF-TNFR2 complex. With these data, we analyzed the structural basis for how TNF can bind to two divergent receptors (TNFR1 and TNFR2) of the same superfamily. This finding contributes to an understanding of the differences between TNFR1 and TNFR2, which may be useful for rationalizing selectivity data and for generating hypotheses to design future TNFR-selective drugs (*11*, *21*). Finally, we discuss the signal initiation mechanism of the TNFR superfamily by analyzing the behavior of the preassembled TNFR2 and TNF-TNFR2 complexes on the surface of a live cell. This is the first report to describe the structural details of a TNF-TNFR2 complex in a crystal and in cells. These findings contribute to our knowledge of members of the TNF superfamily and may provide a new focus for investigation of the signaling machinery of cell surface receptors.

Table 1. Refinement statistics of the TNF-TNFR2 crystal. Ramachandran statistics indicate the fraction of residues in the favored, allowed, and outlier region, respectively, of the Ramachandran diagram as defined by the RAMPAGE program (*65*).

Refinement statistics	
Resolution (Å)	49.96–3.00
Reflections used	43,981
R_{cryst} (%)*	21.3
R_{free} (%)†	28.1
Completeness (%)	99.5
Atoms	
Protein	13,922
Water	11
Co^{2+}	6
RMSD in bonds (Å)	0.004
RMSD in angles (°)	0.759
Ramachandran plot	
Favored region (%)	92.9
Allowed region (%)	6.5
Outlier region (%)	0.6

*$R_{cryst} = \Sigma||F_{obs}| - |F_{calc}||/\Sigma|F_{obs}|$, where F_{obs} and F_{calc} are the observed and calculated structure factors, respectively. †R_{free} is calculated as for R_{cryst}, but for the test set that consists of reflections not used in refinement.

RESULTS

Determination of the structure of the TNF-TNFR2 complex

In a previous report, we obtained a crystal of the TNF-TNFR2 complex belonging to the space group $P2_12_12_1$, as well as preliminary x-ray diffraction data to 2.95 Å (*38*). Here, we solved the structure of the TNF-TNFR2 complex by molecular replacement with the crystal structure of another TNF mutant that we described previously [Protein Data Bank (PDB) code 2e7a] (*39*). Diffraction data sets at 3.0 Å were used in refinements, and the final *R*-factor was 21.3% (with a free *R*-factor of 28.1%) (Table 1). Although we used mutTNF Lys (−) (a lysine-deficient mutant of human TNF that is fully active) (*40*) as the TNF molecule in the TNF-TNFR2 complex (*38*), it was confirmed that mutTNF Lys (−) in the TNF-TNFR2 complex retained almost the same structure as that of wild-type TNF [root mean square deviations (RMSDs) of 0.94 Å for 420 Cα atoms].

We found that the asymmetric unit in the crystal contained two copies of the TNF-TNFR2 complex, which formed an interlocking dimer (two trimers of TNF and six monomers of TNFR2) (Fig. 1, A and B). In this interlocking dimer, CRD2-CRD4 interactions were mainly observed between opposite TNFR2 molecules (Fig. 1, C and D). We observed a potential intermolecular hydrogen bond between Asp^{81} in CRD2 and the amido NH group near Thr^{151} in CRD4 (Fig. 1, E and F), but each TNFR2 mainly interacted through van der Waals contacts. The buried surface area of this interface was relatively extensive (~4300 $Å^2$ for every two copies of the complex), in contrast to ~2500 $Å^2$ in the high-affinity TNF-TNFR2 binding interface. However, according to analytical gel-filtration experiments, the purified TNF-TNFR2 complex in aqueous solution is 110 kD (*38*), which suggests that the TNF-TNFR2 complex contains one trimer of TNF (51 kD) and three monomers of TNFR2 (19 kD each) in aqueous solution. Moreover, the position of the C terminus of TNFR2 suggested that this interlocking dimer would be difficult to form on the cell surface (Fig. 1C). Therefore, we suggested that the formation of such interlocking dimers was a result of crystal packing.

Nonetheless, previous studies showed that mutation of Met^{174} of TNFR2 to Arg, which is referred to as the "M196R polymorphism," is associated with the presence of soluble TNFR2 in the serum (*41*) and autoimmune diseases, such as systemic lupus erythematosus (*42*, *43*). The crystal packing of TNFR2 showed that Met^{174} was located near Arg^{77} of other TNFR2 molecules (Fig. 1, E and F), which suggests that the mutant Arg^{174} residue influences the interaction between the CRD2 of one TNFR2 molecule and the CRD4 of another TNFR2 molecule in the crystal. Although previous gel-filtration analysis suggested that this interlocking dimer was formed by crystal packing, the report on the mutation of Met^{174} in TNFR2 suggests that the interlocking dimer might form only under the specific condition in which TNFR2 is soluble.

TNFR2 structure

The structures of the extracellular domains of members of the TNFR superfamily are composed of CRDs that typically contain six cysteine residues that form three disulfide bonds (*23*). TNFR1 and TNFR2 contain four CRDs, termed CRD1 through CRD4 (Fig. 2A). CRD1 (also known as PLAD) is essential for forming the TNFR self-complex on the cell surface (*33*). CRD2 and CRD3 are known as TNF-binding domains (*23*), whereas the function of CRD4 remains unclear.

Through comparison of the structures of TNFR2 and TNFR1, together with alignment of their corresponding sequences, we found that CRD1 and CRD2 were topologically and structurally similar in both receptors (Fig. 2B). These CRDs contained the modules A1 and B2, which are typically observed in conventional members of the TNFR superfamily (*44*),

such as the structurally determined TNFR1 (*23*), DR5 (*26–28*), and OX40 (*29*) proteins. The A1 module contains a single disulfide bond, whereas the B2 module contains two disulfides, in a consensus sequence pattern. Of note, and different from the CRD3 of TNFR1, the CRD3 of TNFR2 contained the A2 module that is observed in a certain type of TNFR superfamily members, such as the CD30, CD40, and 4-1BB proteins (*44*). Because these TNFR superfamily members have not been structurally identified yet, our structure of the TNF-TNFR2 complex is the first to show the structure of the A2 module. The A2 module in TNFR2 contained two disulfides that were linked in a 1-4, 2-3 topology (Fig. 2C). The 2-3 disulfide (between Cys^{104} and Cys^{112}) contributed to deflect a β-turn motif that was near the ligand-binding region (Fig. 2D), similar to the structure predicted from the A2 module in a viral protein homologous to TNFR2 (*45*). As a result of this disulfide bond, a gap between CRD2 and CRD3 in TNFR2 was buried in the structure (region 1 in Fig. 2, D and E). The location of Arg^{77} in the CRD2 of TNFR1, which is thought to be essential for binding to TNF (*23*), was compensated by Arg^{113} of the TNFR2 CRD3 in the TNF-TNFR2 structure. This structural difference between TNFR1 and TNFR2 was thought to depend on the diversity of their modules.

We observed another structural difference between TNFR1 and TNFR2 in region 2 (Fig. 2, D and E). A loop structure in TNFR1, which is reported to constitute the ligand-binding region (*23*), consisted of five residues in TNFR1 (Arg^{77} to Gly^{81}) but only three residues in TNFR2 (Ser^{79} to Asp^{81}) (Fig. 2B). The shorter loop structure of TNFR2 was further from the molecular surface of TNF ligand compared with that of TNFR1 as described below.

The TNF-TNFR2 complex

We found that TNF formed a central homotrimer around which three TNFR2 molecules were bound, similar to the known structures of other TNF superfamily members, including LT-α–TNFR1 (*23*), TRAIL-DR5 (*26–28*), and OX40L-OX40 (*29*) (Fig. 3, A and B). The structure of the TNF-TNFR2 complex revealed that the TNFR1-binding region of TNF overlapped with its TNFR2-binding region, as previously predicted (*46*). One TNFR2 molecule interacted with two TNF molecules, as is the case for the LT-α–TNFR1 complex. The core of the interface between TNFR2 and TNF was separated into two regions, termed regions 3 and 4 (Fig. 3, B to D). Region 3 consisted of the A1 module of CRD2, whereas region 4, which was near regions 1 and 2, consisted of the B2 module of CRD2 and the A2 module of CRD3. Comparison of the electrostatic surface potentials of TNFR1 and TNFR2 showed that they were different despite sharing the same binding partner (Fig. 3, C and D). In the interface of TNFR2 region 3, acidic amino acid residues (Asp^{54}, Glu^{57}, and Glu^{70}) were clustered, forming a more negatively charged surface than that of TNFR1. Moreover, in region 4 of TNFR2, the molecular surface was different from that of TNFR1, possibly as a result of diversity in the modules present (Fig. 2B). This structural feature contributed to the exposure of basic amino acids (Arg^{77}, Lys^{108}, and Arg^{133}) at the binding interface, which generated a positively charged surface on TNFR2.

Although a cobalt ion (Co^{2+}) from the crystallization reagent was observed at all six interfaces in the asymmetric unit (Fig. 4A), Arg^{31} of TNF appeared to interact with the negatively charged region 3 on the surface of TNFR2 (Fig. 4B). By contrast, our model of the TNF-TNFR1 complex, constructed from the structure of the LT-α–TNFR1 complex, indicated that the interaction between Arg^{31} and the TNFR1 might be weak, because of the neutral charge of region 3 (Fig. 4C). Indeed, a previously reported R31D mutant of TNF displays a marked loss of affinity for TNFR2 while retaining affinity for TNFR1 (*47*). Therefore, these results suggest that this electrostatic interaction between Arg^{31} of TNF and TNFR is more important for the TNF-TNFR2 complex than for that of TNF and TNFR1. We found that Arg^{32} of TNF was located in a position that enabled a potential hydrogen bond to be formed with Ser^{73} of TNFR2 and that it seemed to interact with Ser^{72} of TNFR1 in the same way. Therefore, we suggest that Arg^{32} of TNF contributes equally to the binding of TNF to TNFR1 and TNFR2.

Detail of region 4 showed that Arg^{113} and Arg^{77} of TNFR2 formed close contacts to Asp^{143}, Gln^{149}, and Glu^{23} of TNF, potentially through the formation of hydrogen bonds. Thus, Arg^{113} and Arg^{77} of TNFR2 were important residues for binding to TNF (Fig. 4, E and F). This result is also supported from previous analysis of point mutations of TNF (*46*, *48*, *49*). Meanwhile, Arg^{77} of TNFR1 appeared to interact with Asp^{143} and Gln^{149} of TNF (Fig. 4F). We suggest that Arg^{113} of TNFR2 and Arg^{77} of TNFR1 might have similar roles in binding to TNF (Fig. 4, E and F). This difference regarding arginine residues between TNFR1 and TNFR2 was also indicated earlier (Fig. 2, D and E). The origin of this difference in inter-

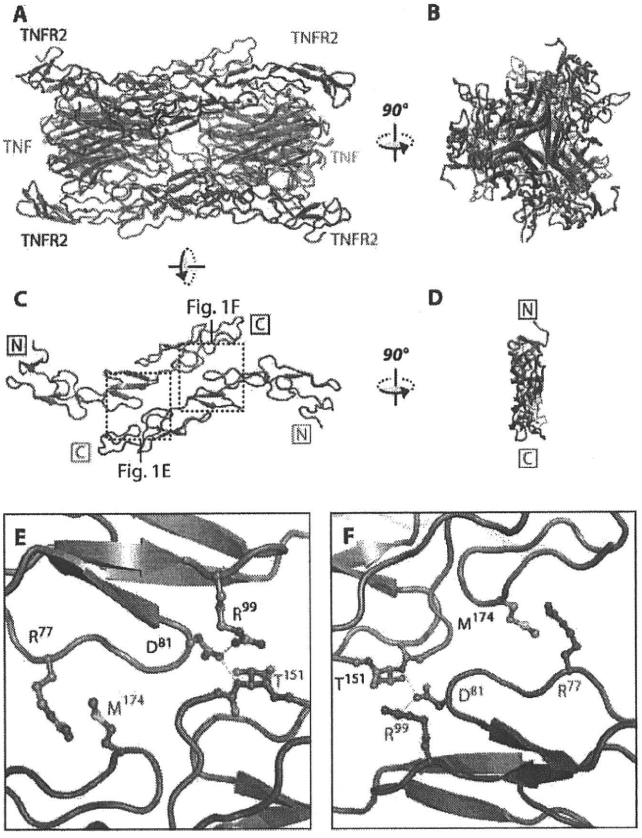

Fig. 1. TNF-TNFR2 complex in the asymmetric unit. Two TNF-TNFR2 complexes are observed in the asymmetric unit (consisting of two TNF trimers and six TNFR2 monomers). TNFR2 molecules from different complexes interact with each other in the crystal. TNF molecules are shown in green and orange; TNFR2 molecules are shown in blue and red. (A and B) Side view (A) and top view (B) of the complexes. (C and D) Side view (C) and top view (D) of the TNFR2-TNFR2 interaction in the crystal. N, N terminus; C, C terminus. (E and F) Details of the TNFR2-TNFR2 interfaces. Close contacts that are suggestive of potential hydrogen bonds are shown as yellow dashed lines.

action was a result of the unique A2 module and the dynamic structural diversity close to regions 1, 2, and 4.

Usefulness of the molecular pocket formulation for the design of TNFR1-selective inhibitors

Differences in the composition of the respective modules together with the diversity in the length of the main chain near the binding interface constitute the basic structural elements that distinguish TNFR1 from TNFR2. These structural considerations could form the basis of the design of receptor-specific drugs. Previous mutational analysis showed that region 1 of TNFR1 and TNFR2 (Fig. 2, D and E) is essential for the interaction with the loop of TNF (amino acid residues 143 to 149) (*46*, *48*, *49*). In this ligand-binding area of TNFR2, the turn motif of CRD3 (Ser^{107} to Cys^{112}) fit to its CRD2 in the presence of the disulfide bond between Cys^{104} and Cys^{112} (Figs. 2D and 5A). By contrast, there was a space between the turn motif of the CRD3 of TNFR1 and the β strand of its CRD2, which resulted in the formation of a molecular pocket specifically on the surface of TNFR1 (Fig. 5B). These observations suggest that this region of TNFR1 constitutes a promising target for the structure-based development of TNFR1-selective drugs.

Another point of interest was observed in region 2. A number of amino acid residues contained in the loop structure of region 2 differ between TNFR1 and TNFR2 (Fig. 2B). In the shorter loop of TNFR2 (residues Ser^{79} to Asp^{81}), there was a space between TNF and the receptor

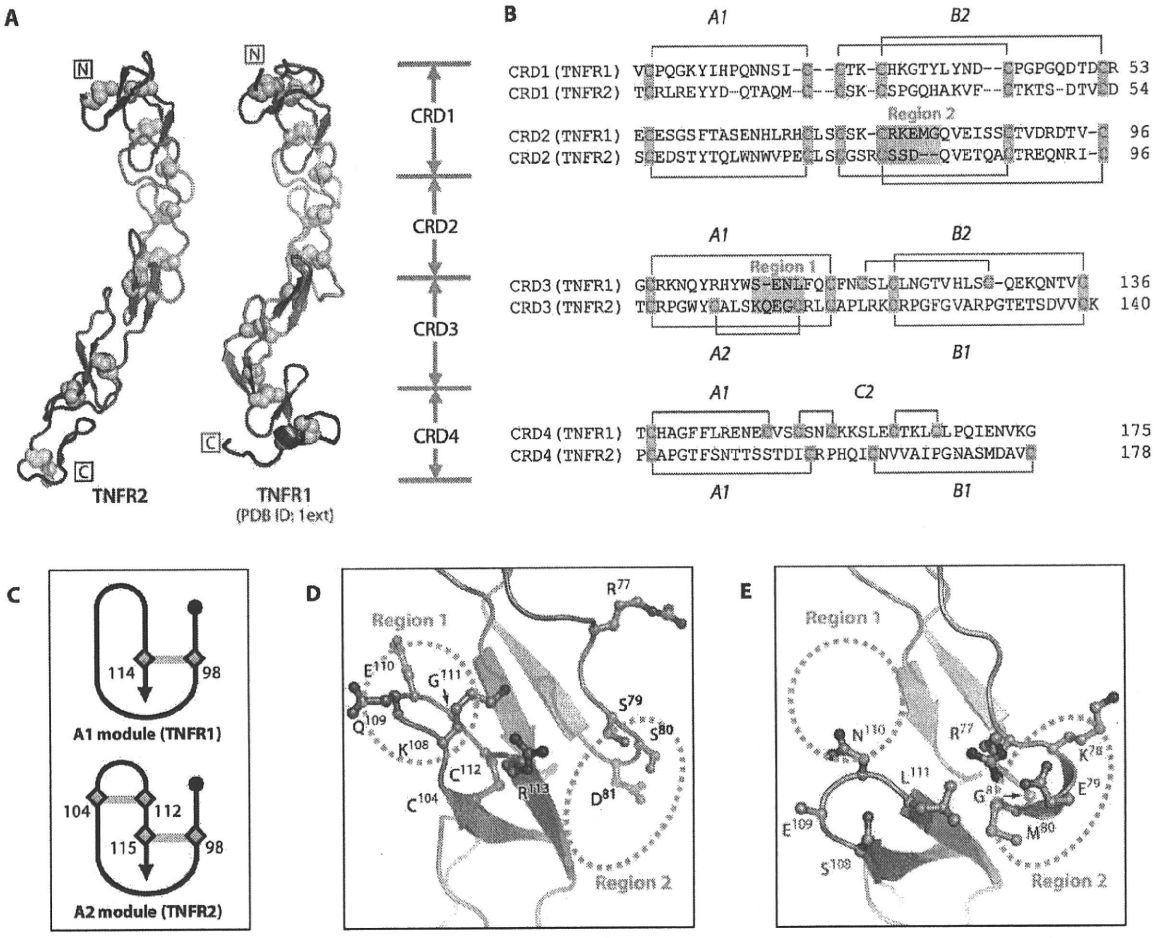

Fig. 2. Basic structure and folding of TNFR2 and TNFR1. (**A**) Structure of the extracellular domain of TNFR2 in blue (PDB ID 3alq) and TNFR1 in red (PDB ID 1ext). Disulfide linkages are shown as green spheres. For a comparison of the basic structures, we superimposed a crystal structure of unbound TNFR1 (CRD1 to CRD3 of PDB ID 1ext) (*55*) onto the structure of TNFR2 (CRD1 to CRD3) with the SUPERPOSE program (*67*) in CCP4i. (**B**) Alignment of the amino acid sequences of TNFR1 and TNFR2. A1, A2, B1, B2, and C2 are the names of the module structures. Cysteine residues are highlighted in green. Differences between the structures of TNFR1 and TNFR2 (regions 1 and 2) are highlighted in orange. The amino acid sequence alignment was performed with the ClustalW program (*68*). Abbreviations for the amino acids are as follows: A, Ala; C, Cys; D, Asp; E, Glu; F, Phe; G, Gly; H, His; I, Ile; K, Lys; L, Leu; M, Met; N, Asn; P, Pro; Q, Gln; R, Arg; S, Ser; T, Thr; V, Val; W, Trp; and Y, Tyr. (**C**) The A1 and A3 modules. There are different modules in the CRD3 regions of TNFR1 and TNFR2. (**D**) Ligand-binding interface of TNFR2. (**E**) Receptor binding interface of TNFR1. To compare the binding interfaces, we superimposed a crystal structure of TNFR1 complexed with LT-α (CRD1 to CRD3 of PDB ID 1tnr) onto the structure of TNFR2 (CRD1 to CRD3) with the SUPERPOSE program. The side chain of Glu^{109} is missing in the structure of TNFR1 (PDB ID 1tnr). Structural differences between TNFR1 and TNFR2 (regions 1 and 2) are also highlighted by orange dashed circles.

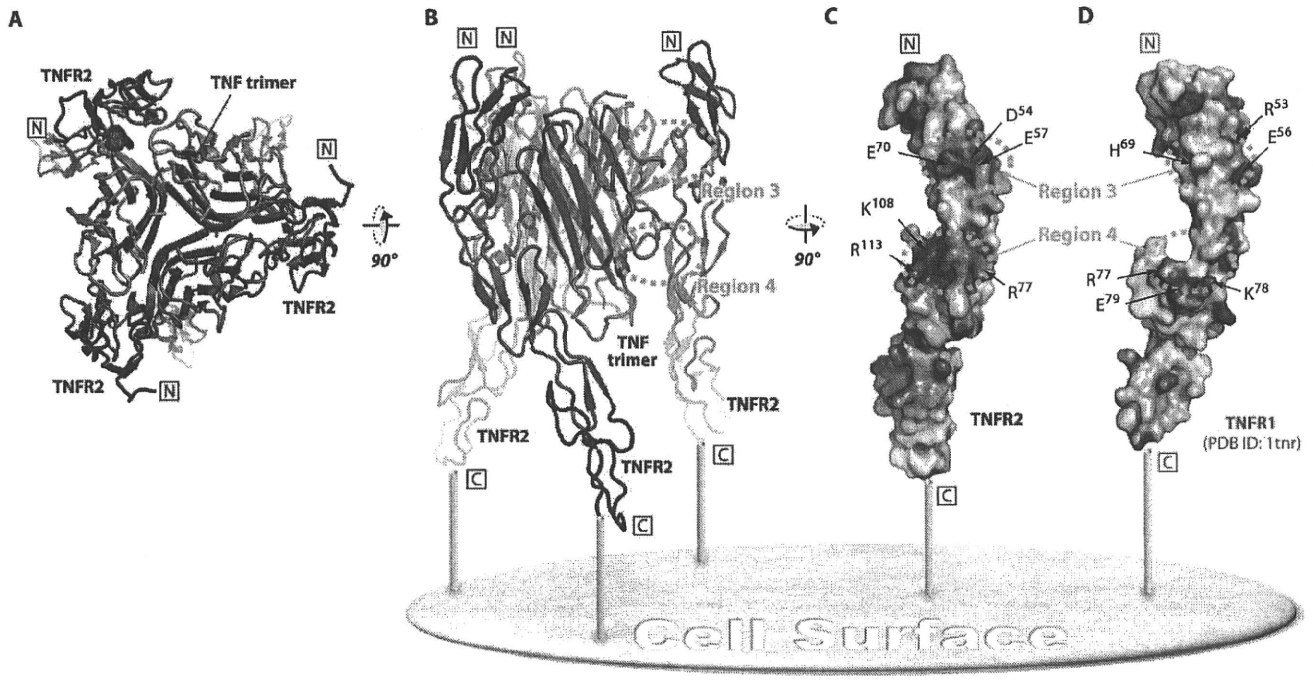

Fig. 3. Electrostatic surface potentials on the binding interfaces of TNFR2 and TNFR1. (A and B) Top view (A) and side view (B) of TNF-TNFR2 complexes (PDB ID 3alq). The TNF trimer is in green and the TNFR2 monomer is in blue. The binding regions (regions 3 and 4) are highlighted by orange, dashed circles. (C) Electrostatic surface potential of TNFR2. (D) Electrostatic surface potential of TNFR1 (PDB ID 1tnr). Each electrostatic surface potential was calculated with the GRASP program (*69*). Electrostatic charges (red indicates a negative charge, blue indicates a positive charge) are shown between $\pm 8k_BT$, where k_B is the Boltzmann constant and T is the absolute temperature.

(Fig. 5C). By contrast, the longer loop structure of TNFR1 (residues Arg^{77} to Gly^{81}) was predicted to bind to TNF across a wide surface area by van der Waals contacts (Fig. 5D). This interaction is also observed in the structure of the LT-α–TNFR1 complex (*23*). These observations suggest that the loop motif in TNFR1 could be a focal point for creating new drugs that specifically inhibit the interaction between TNF and TNFR1.

A TNF-TNFR2 complex on the cell surface

Previous studies have confirmed that some members of the TNFR superfamily form a self-complex through their CRD1 (PLAD) regions at the cell surface, which also suggests that stimulation by ligand of these assemblies is necessary for efficient signaling (*32*, *33*). In the crystal structure of the TNF-TNFR2 complex, however, the CRD1 regions were separated from each other by >30 Å, which is too far to enable an interaction to occur. This phenomenon is also observed in other TNF-TNFR complexes (*23*, *26*–*29*). These apparently contradictory observations suggest that the binding of the TNF ligand induces a dynamic behavior in the TNFR self-complex that may trigger signal initiation.

To understand the state of TNFR2 at the cell surface, we transfected human embryonic kidney (HEK) 293T cells with plasmids encoding hemagglutinin (HA)–tagged wild-type TNFR2 (HA-wtTNFR2), TNFR2 lacking its PLAD (HA-TNFR2ΔPLAD), or TNFR2 lacking its intracellular domain (HA-TNFR2ΔCD). To identify self-complexes formed through PLAD-mediated interactions, we used the thiol-cleavable, membrane-impermeant, chemical cross-linker 3,3′-dithiobis(sulfosuccinimidyl propionate) (DTSSP), as described in a previous report (*33*). We performed Western blotting analysis of purified membrane fractions with antibody against HA to detect cross-linked, HA-tagged TNFR2 molecules. We observed a band corresponding to monomeric TNFR2 with a molecular mass of 65 kD (Fig. 6A, lanes 1 to 4). We also detected self-complexes of TNFR2 in the absence of TNF with molecular sizes about two or three times greater (130 or 195 kD) (Fig. 6A, lane 1), consistent with previous reports (*33*). Furthermore, analysis with high–molecular mass markers and a low-density polyacrylamide gel enabled us to identify a band of TNFR2 with a molecular mass of >1000 kD in samples treated with TNF (Fig. 6A, lane 2). These complexes were reduced to monomeric proteins by cleaving the cross-linker with dithiothreitol (DTT) (Fig. 6A, lanes 3 and 4). A similar experiment with cells transfected with plasmid encoding HA-TNFR2ΔPLAD revealed that the formation of TNFR2 self-complexes in the presence and absence of TNF was inhibited by the deletion of PLAD (Fig. 6A, lanes 5 and 6). In addition, treatment with TNF did not induce a shift in the band corresponding to HA-TNFR2ΔPLAD (Fig. 6A, lane 6), suggesting that most of the TNF did not bind to TNFR2 without PLAD at the cell surface. A previous report showed that deletion of the PLAD from TNFR1 markedly decreases the amount of TNF that binds to cell surface TNFR1 (*33*). Thus, our result suggests that the binding of TNF to TNFR2 is also disrupted by the deletion of the PLAD from TNFR2. In experiments with cells transfected with plasmid encoding HA-TNFR2ΔCD, we showed that this mutant TNFR could still form self-complexes (Fig. 6A, lane 9); however, the band corresponding to HA-TNFR2ΔCD did not shift upon treatment with TNF (Fig. 6A, lane 10). These results suggest that self-complexes of TNFR2 are formed through its PLAD on the surface of cells and that the stimulation of TNF was important for the formation of high–molecular mass aggregates of TNFR2.

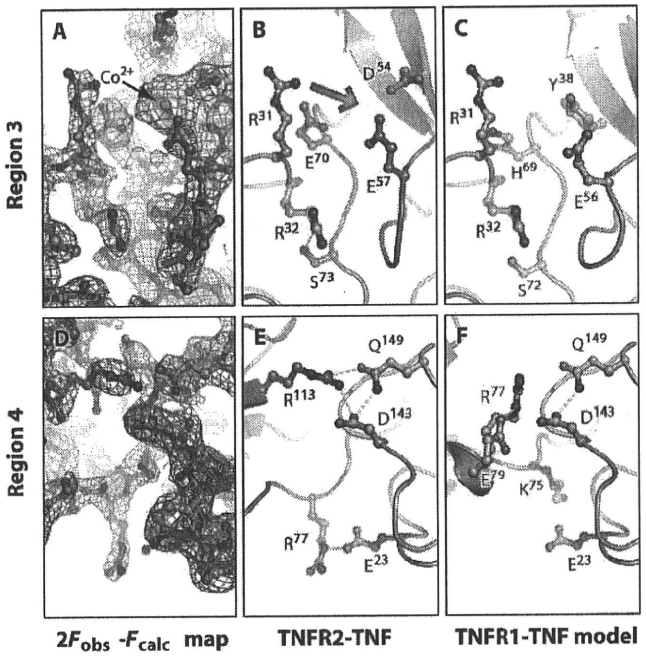

Fig. 4. Difference in the mode of binding of TNF to TNFR1 and TNFR2. Details of the ligand-receptor binding interfaces of TNF-TNFR are shown. (A and D) $2F_{obs} - F_{calc}$ map of the TNF-TNFR2 complex contoured at 1.0 σ. (B and E) The TNF-TNFR2 complex. The predicted interaction between R31 of TNF and the acidic surface of TNFR2 (consisting of D54, E57, and E70) is shown as a green arrow. (C and F) The TNF-TNFR1 model complex. To construct the TNF-TNFR1 model complex, we superimposed the LT-α portion of the LT-α–TNFR1 complex (PDB ID 1tnr) (*23*) onto the TNF portion of the TNF-TNFR2 structure. TNF is in green; TNFR1 is in red; TNFR2 is in blue; the $2F_{obs} - F_{calc}$ map is represented by the pink mesh. Close contacts that are suggestive of potential hydrogen bonds are represented by yellow dashed lines.

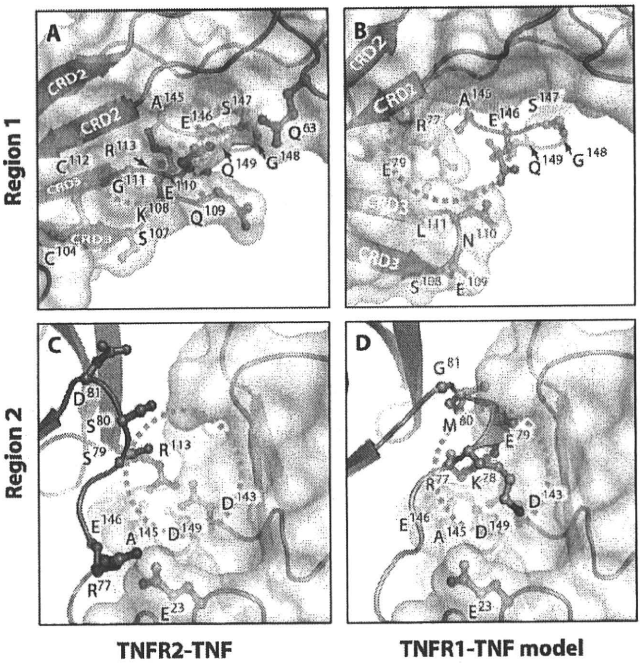

Fig. 5. TNF-TNFR complexes contain a molecular pocket. Difference in the basic structures of TNFR1 and TNFR2. (A and C) The TNF-TNFR2 complex. (B and D) The TNF-TNFR1 model complex, which was constructed as described in Fig. 4. TNF is in green; TNFR1 is in red; TNFR2 is in blue. The β strands of CRD2 and CRD3 are indicated by white text. The side chain of Glu^{109} is missing in the structure of TNFR1 (PDB ID 1tnr). We observed that a distinct molecular pocket was formed in (B) and (C), which is highlighted by an orange dashed circle.

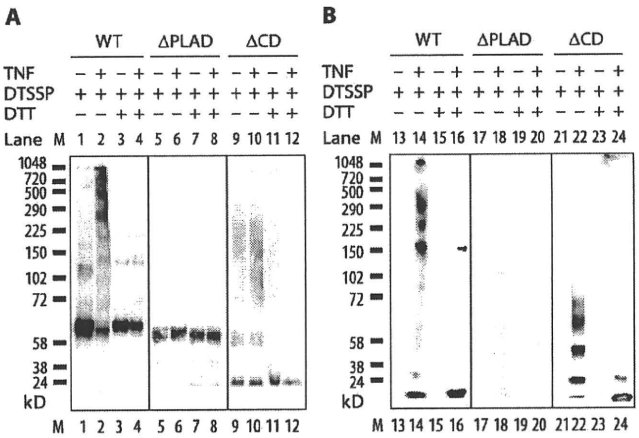

Fig. 6. Formation of TNF-TNFR2 aggregates on the cell surface. (A and B) TNF-TNFR2 complexes in the plasma membrane of transfected HEK 293T cells were detected by Western blotting analysis with antibodies against (A) the HA epitope and (B) TNF. This result was confirmed by three independent experiments for each group. Predicted molecular masses of related molecules are as follows: HA-wtTNFR2 monomer, 65 kD; HA-wtTNFR2 dimer, 130 kD; HA-wtTNFR2 trimer, 195 kD; TNF monomer, 17 kD; TNF trimer, 51 kD; HA-TNFR2ΔPLAD monomer, 60 kD; HA-TNFR2ΔCD monomer, 25 kD.

We also analyzed the same samples by Western blotting with an antibody against TNF (Fig. 6B). We observed high–molecular mass, TNF-specific bands of >150 kD in samples containing HA-wtTNFR2 and TNF (Fig. 6B, lane 14), but saw only monomeric TNF (17-kD band) under reducing conditions (Fig. 6B, lane 16). This result suggests that TNF molecules were contained in the aggregates of TNFR2 that we observed earlier (Fig. 6A, lane 2). In similar experiments with cells containing HA-TNFR2ΔPLAD, we did not observe TNF-specific bands in any group (Fig. 6B, lanes 17 to 20), indicating that TNF bound rarely to TNFR2ΔPLAD, as was predicted from our earlier results (Fig. 6A). These findings suggest that TNF bound to the PLAD-dependent self-complex of TNFR2 and that the PLAD was a key domain in forming a TNF-TNFR2 aggregate on the cell surface. We could not observe TNF within the self-complex of HA-TNFR2ΔCD (Fig. 6, A and B), indicating that the intracellular domain of TNFR2 also played an important role in forming the TNF-TNFR2 aggregate on the cell surface.

DISCUSSION

Here, we described the first crystal structure of the TNF-TNFR2 complex at a resolution of 3.0 Å. TNF formed a central homotrimer around which were bound three TNFR2 molecules. This overall arrangement was similar

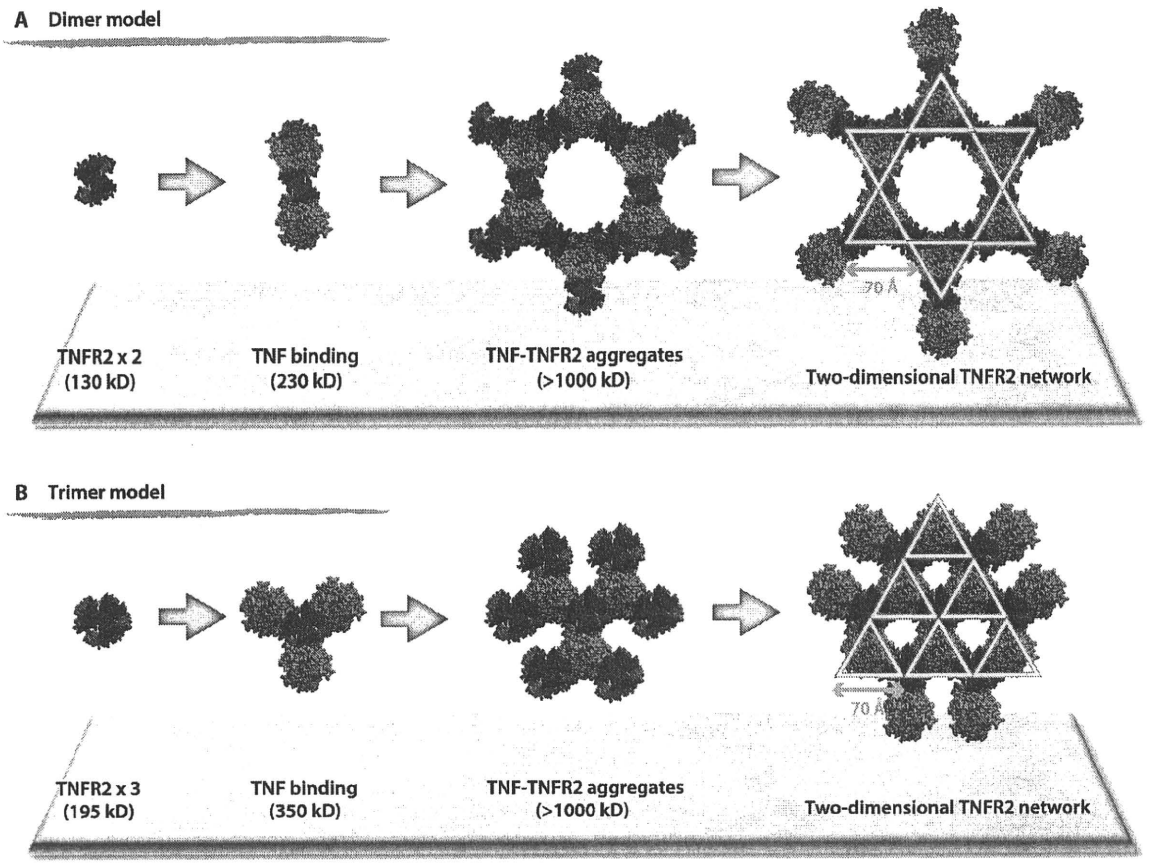

Fig. 7. Structural feasibility of a two-dimensional network model for the initiation of signals through TNFR2. (A and B) Top views of (A) the dimer model and (B) the trimer model of a two-dimensional network of TNFR2. TNFR2 molecules can interact with each other through PLAD-PLAD interactions (deep blue) at the cell surface. TNF trimers can bind around the self-complex of TNFR2. The binding of TNF to TNFR2 may link it to other TNFR2 self-complexes through alternative binding sites, which could result in the formation of a two-dimensional TNF-TNFR2 network. TNF-TNFR2 networks in the dimer and trimer models would maintain six- and threefold symmetry, respectively. These arrangements of TNF-TNFR2 complexes appear to be structurally realistic in both models. The extracellular domain of TNFR2 is in blue and TNF is in green.

to those of other members of the TNF superfamily, including LT-α–TNFR1 (*23*), TRAIL-DR5 (*26–28*), and OX40L-OX40 (*29*) (Fig. 3). However, our determination of the crystal structure of TNFR2 revealed subtle differences with that of TNFR1. The basic structure of TNFR2 differed from that of TNFR1 mainly as a result of variation in the configuration of the folding module. These structural differences altered the mode of ligand recognition of each receptor (Figs. 4 and 5). The results contribute to our understanding of how TNF is able to discriminate between the common binding areas of these two different receptors. In addition, we have already created many mutant TNFs that exhibit different receptor selectivities (*39*, *46*, *50*, *51*). The structures of these mutants and TNF-TNFR complexes are potentially useful to analyze "consensus" information that is essential for the TNF-TNFR interaction (*52*). Such information will be useful in the future for enhancing accuracy in the rational design of new drugs, such as TNFR-selective inhibitors.

We also revealed the formation of an aggregate of TNFR2 on the cell surface (Fig. 6). These aggregates contained both TNF and TNFR2, which indicated that an aggregate of TNF-TNFR2 complexes (>1000 kD) was present on the cell surface. This result was observed in cells transfected to express TNFR2 at the surface and needs to be confirmed by another experimental method in primary cells in the future. However, the importance of such TNF-TNFR2 aggregates in the initiation of TNFR signaling can also be predicted from a previous report on TNF heterotrimers that contained inactive, mutant TNF molecules that acted as dominant-negative TNF because of their lack of trivalent binding potency (*53*).

The HA-TNFR2ΔCD mutant formed a self-complex, but not an aggregate of TNF and TNFR2. Because the structure of the intracellular domain of TNFR2 is still unknown, we are unable to discuss the implications of these findings in detail. Nonetheless, we can speculate that the arrangement of the intracellular domain of TNFR2 might be important for the formation of aggregates of TNF and TNFR2 on the cell surface. Our deletion experiment with HA-TNFR2ΔPLAD indicated that the TNFR2 self-complex forms through PLAD-PLAD interactions, resulting in generation of the TNF-TNFR2 aggregate; however, despite the possibility of the formation of the TNF-TNFR2 complex through PLAD-mediated interactions, we observed that the PLADs of each TNFR2 were dissociated in the crystal structure (Fig. 3). To resolve this apparent contradiction in TNF-mediated signal initiation, we used a structure-based hypothesis based on information concerning our observation of TNF-TNFR2 aggregates of >1000 kD and the crystal structure of TNFR2.

Regarding our prediction of the configuration of the TNFR on the cell surface, previous studies showed that two types of ligand-free TNFR1 proteins form dimers in crystal structures, which are termed parallel dimers at pH 7.5 (*54*) and antiparallel dimers at pH 3.7 (*55*). The TNFR1 parallel dimer forms through PLAD-PLAD interactions in the crystal, and it has been speculated that such a dimer may also be formed on the cell surface (*54*); however, our data (Fig. 6) and another report (*33*) suggest that TNFR1 and TNFR2 form a self-complex as homodimers or homotrimers on the cell surface. Given that the stoichiometry of the TNFR2 self-complex is unclear, these findings imply two possible models for the complex (dimer and trimer models) (Fig. 7). In these models, two or three TNF trimers bind around a central dimer or trimer of TNFR2 molecules, respectively. Other self-complexes of TNFR2 are subsequently recruited to bind around the TNFs, generating an aggregate of TNF-TNFR2 in a two-dimensional network on the cell surface. TNF-TNFR2 networks in the dimer and trimer models would maintain six- and threefold symmetries, respectively. The crystal structure of the TNF-TNFR2 complex suggests that these arrangements of complexes appear to be structurally realistic in both models. This structural feasibility will strengthen a predicted two-dimensional network model described previously (*54*, *56*). Finally, expansion of the network may influence the arrangement of the intracellular domains of TNFR2, thereby possibly inducing the recruitment of intracellular molecules, such as TNFR-associated factor 2 (TRAF2) in TNFR2 signaling.

With respect to TRAF2, we can speculate about its intracellular behavior after the formation of the TNF-TNFR2 aggregate. TRAF2 is essential for TNFR2-mediated signaling. Indeed, the structure of a complex of the C-terminal domain of TRAF2 and a peptide from the intracellular domain of TNFR2 has been reported (*57*). The C-terminal domain of TRAF2 forms a trimer that binds to the intracellular domains of three TNFR2 molecules (*57*); however, there is no structural difference between the peptide-bound form and the unbound form. Therefore, it was unclear how TRAF2 transduces a signal to downstream molecules. The crystal structure of the N-terminal domain of TRAF6, which is homologous to TRAF2, has been solved (*58*). The structure shows that the N-terminal domains of TRAF6 are complexed to each other, suggesting that this interaction forms part of its signaling mechanism. Together, these findings suggest that the TNF-TNFR2 network might organize the intracellular domains of TNFR2 and induce the recruitment of TRAF2, which would result in a TRAF2-TRAF2 intermolecular interaction that is needed for signal transduction. Although this structure-based hypothesis needs to be confirmed by other experiments (for example, role of the intracellular domain and the use of a non–cross-linking methodology such as the direct observation of cell surface complexes with an electron microscope), we suggest that it might provide a new direction for solving the enigma concerning the mechanism of signal initiation of TNFR superfamily members.

The TNF-TNFR2 structures revealed in this report show the diversity in the molecular basis of TNF-TNFR recognition and provide a better understanding of the mechanism of signal initiation by members of the TNFR superfamily. We hope to develop the next generation of therapeutics with an approach based on our structural data, such as new drugs that can selectively inhibit the interaction between one type of TNF-TNFR complex or the formation of one specific type of TNF-TNFR aggregate.

MATERIALS AND METHODS

Data collection and refinement

The complex of amino acid residues 1 to 157 of human TNF (which corresponds to residues 77 to 233 in UniProt P01375) and residues 11 to 183 in human soluble TNFR2 (which corresponds to residues 33 to 205 in UniProt P20333) were prepared as previously described (*38*). The human TNF used in this experiment was mutTNF Lys (−), a lysine-deficient, hexamutant TNF (K11M, K65S, K90P, K98R, K112N, and K128P) with full bioactivity (*40*). This TNF molecule was expressed as inclusion bodies in *Escherichia coli* and refolded as described previously (*38*, *40*). Recombinant human soluble TNFR2 was purchased from PeproTech Inc. (catalog no. 310-12). This TNFR2 molecule was also expressed in *E. coli*. Crystallization and x-ray diffraction experiments were performed as previously described (*38*). Diffraction data were collected at SPring-8 in Harima and Photon Factory in Tsukuba, Japan. The data were indexed, integrated, and scaled with HKL2000 software (*59*). The data set used for structural analysis was collected in BL41XU of SPring-8. Molecular replacement was performed by the MOLREP program (*60*) in CCP4i (*61*) with the structure of the TNF mutant described in our previous report (*39*) (PDB code 2e7a) as a search model. The model from molecular replacement was refined with crystallography and nuclear magnetic resonance (NMR) system (CNS) software (*62*). The Cα chains of TNFR2 molecules were manually traced on the basis of the structure of TNFR1 (PDB code 1tnr) with the Coot program (*63*) in CCP4i. The final structure was refined by the PHENIX program (*64*), and validation of the final model was performed with the RAMPAGE program (*65*) in CCP4i. Data collection statistics (at a resolution of 2.95 Å) were described previously (*38*), and the final structure was refined at a resolution of 3.0 Å. Refinement statistics are given in Table 1. The diffraction data set has a poor R_{merge} value of 0.18, as reported in a previous paper (*38*). This might arise from high and anisotropic mosaicity of the crystals. The gap (6.7%) between the values of R and R_{free} is slightly larger than the 5% that is accepted as no overfitting, which might result from flexible loops with poor electron densities. However, because almost all of the electron densities were interpretable (as shown in Fig. 4, A and D), the overall structure is of sufficient quality to characterize the TNFR2 structure and reveal the recognition mechanism between TNF and TNFR2. All molecular graphics were rendered by PyMOL program (*66*).

Plasmid construction

Plasmids encoding TNFR2 were constructed with the help of a previous report (*33*). Briefly, the leader sequence and the first 10 amino acid residues of full-length, wild-type TNFR2 (wtTNFR2: residues 1 to 32 in UniProt P20333) were connected to the HA epitope tag (YPYDVPDYA) at its C terminus to generate an HA tag fused to the N terminus of TNFR2. Complementary DNAs (cDNAs) of HA-wtTNFR2 (encoding residues 1 to 32–HA–residues 33 to 461 in UniProt P20333), HA-TNFR2ΔPLAD (encoding residues 1 to 32–HA–residues 77 to 461 in UniProt P20333), and HA-TNFR2ΔCD (encoding residues 1 to 32–HA–residues 33 to 287 in UniProt P20333) were amplified and directly cloned into pcDN3.1D/V5-His-TOPO vectors (Invitrogen Corp.). Primers 1 (5′-CACCATGGCGCCCGTCGCCGTCTGGGCCGCGCTGGCCGTCGGACTGGAGCTCTGGGCTGCGGCGCACGCCTTGCCCGCCCAGGTGGCATTTACACCCTACTACCCCTATGATGTGCCAGACTACGCCGCCCCGGAGCCCGGGAGCACATGC-3′) and 3 (5′-TTAACTGGGCTTCATCCCAGCATC-3′) were used to amplify HA-wtTNFR2, whereas primers 2 (5′-CACCATGGCGCCCGTCGCCGTCTGGGCCGCGCTGGCCGTCGGACTGGAGCTCTGGGCTGCGGCGCACGCCTTGCCCGCCCAGGTGGCATTTACACCCTACGCCCTACCCCTATGAGGTGCCAGACTATCCTGTGAGGACAGCACATACACC-3′) and 3 were used to amplify HA-TNFR2ΔPLAD cDNA. Primers 1 and 4 (5′-TCACACCTGGGTCATGATGACACAGTT-3′) were used for the amplification of HA-TNFR2ΔCD.

Expression and cross-linking of TNFR2 at the cell surface

HEK 293T cells were cultured in Dulbecco's modified Eagle's medium (DMEM) (Wako Pure Chemical Industries Ltd.), containing 10% fetal

bovine serum at 37°C under 5% CO_2. Cells were transfected with plasmids encoding HA-wtTNFR2, HA-TNFR2ΔPLAD, or HA-TNFR2ΔCD with Lipofectamine LTX and Plus reagent (Invitrogen). After incubation for 6 hours at 37°C under 5% CO_2, TNFR2 proteins were expressed on the surface of the HEK 293T cells. For cells treated with TNF, recombinant human TNF (R&D Systems Inc.) was added to the cells at a final concentration of 5 μg/ml, and the cells were then incubated at 4°C for 1 hour. Cells were scraped from the culture dish and incubated in 1 mM DTSSP (Thermo Fisher Scientific Inc.) for 30 min at room temperature to cross-link cell surface TNFR2 complexes. The cross-linking reaction was terminated by the addition of 20 mM tris-HCl (pH 7.4). Membrane proteins, which contained cell surface TNFR2 complexes, were purified with the Plasma Membrane Protein Extraction Kit (BioVision).

Western blotting analysis

Purified membrane proteins were mixed with an equal volume of Laemmli sample buffer (Bio-Rad Laboratories Inc.) with or without 50 mM DTT (Thermo Fisher Scientific). The samples were subjected to SDS–polyacrylamide gel electrophoresis (SDS-PAGE) with a 3 to 10% gradient polyacrylamide gel (ATTO Corp.). Proteins were then transferred onto a polyvinylidene difluoride (PVDF) membrane (GE Healthcare Bio-Sciences Corp.). We used antibody against the HA epitope (Abcam Inc.) and horseradish peroxidase (HRP)–conjugated antibody against mouse immunoglobulin G (IgG) (GE Healthcare Bio-Sciences) to detect HA-wtTNFR2, HA-TNFR2ΔPLAD, and HA-TNFR2ΔCD proteins. To detect TNF, we used antibody against human TNF (Genzyme Corp.) and HRP-conjugated antibody against mouse IgG. Specific bands were visualized with the ECL Plus reagent (GE Healthcare Bio-Sciences). To estimate the molecular mass of large complexes, we used high–molecular weight markers (NativeMark and HiMark HMW standard; Invitrogen).

REFERENCES AND NOTES

1. B. B. Aggarwal, Signalling pathways of the TNF superfamily: A double-edged sword. *Nat. Rev. Immunol.* **3**, 745–756 (2003).
2. W. M. Kooloos, D. J. de Jong, T. W. Huizinga, H. J. Guchelaar, Potential role of pharmacogenetics in anti-TNF treatment of rheumatoid arthritis and Crohn's disease. *Drug Discov. Today* **12**, 125–131 (2007).
3. P. Rutgeerts, G. Van Assche, S. Vermeire, Optimizing anti-TNF treatment in inflammatory bowel disease. *Gastroenterology* **126**, 1593–1610 (2004).
4. M. Feldmann, R. N. Maini, Lasker Clinical Medical Research Award. TNF defined as a therapeutic target for rheumatoid arthritis and other autoimmune diseases. *Nat. Med.* **9**, 1245–1250 (2003).
5. M. G. Tansey, D. E. Szymkowski, The TNF superfamily in 2009: New pathways, new indications, and new drugs. *Drug Discov. Today* **14**, 1082–1088 (2009).
6. R. O. Williams, M. Feldmann, R. N. Maini, Anti-tumor necrosis factor ameliorates joint disease in murine collagen-induced arthritis. *Proc. Natl. Acad. Sci. U.S.A.* **89**, 9784–9788 (1992).
7. G. J. Thorbecke, R. Shah, C. H. Leu, A. P. Kuruvilla, A. M. Hardison, M. A. Palladino, Involvement of endogenous tumor necrosis factor α and transforming growth factor β during induction of collagen type II arthritis in mice. *Proc. Natl. Acad. Sci. U.S.A.* **89**, 7375–7379 (1992).
8. J. S. Lubel, A. G. Testro, P. W. Angus, Hepatitis B virus reactivation following immunosuppressive therapy: Guidelines for prevention and management. *Intern. Med. J.* **37**, 705–712 (2007).
9. J. J. Gomez-Reino, L. Carmona, V. R. Valverde, E. M. Mola, M. D. Montero, BIOBADASER Group, Treatment of rheumatoid arthritis with tumor necrosis factor inhibitors may predispose to significant increase in tuberculosis risk: A multicenter active-surveillance report. *Arthritis Rheum.* **48**, 2122–2127 (2003).
10. S. L. Brown, M. H. Greene, S. K. Gershon, E. T. Edwards, M. M. Braun, Tumor necrosis factor antagonist therapy and lymphoma development: Twenty-six cases reported to the Food and Drug Administration. *Arthritis Rheum.* **46**, 3151–3158 (2002).
11. D. Faustman, M. Davis, TNF receptor 2 pathway: Drug target for autoimmune diseases. *Nat. Rev. Drug Discov.* **9**, 482–493 (2010).
12. L. Mori, S. Iselin, G. De Libero, W. Lesslauer, Attenuation of collagen-induced arthritis in 55-kDa TNF receptor type 1 (TNFR1)-IgG1-treated and TNFR1-deficient mice. *J. Immunol.* **157**, 3178–3182 (1996).
13. M. Leist, F. Gantner, S. Jilg, A. Wendel, Activation of the 55 kDa TNF receptor is necessary and sufficient for TNF-induced liver failure, hepatocyte apoptosis, and nitrite release. *J. Immunol.* **154**, 1307–1316 (1995).
14. E. Y. Kim, J. J. Priatel, S. J. Teh, H. S. Teh, TNF receptor type 2 (p75) functions as a costimulator for antigen-driven T cell responses in vivo. *J. Immunol.* **176**, 1026–1035 (2006).
15. E. Y. Kim, H. S. Teh, TNF type 2 receptor (p75) lowers the threshold of T cell activation. *J. Immunol.* **167**, 6812–6820 (2001).
16. M. Grell, F. M. Becke, H. Wajant, D. N. Mannel, P. Scheurich, TNF receptor type 2 mediates thymocyte proliferation independently of TNF receptor type 1. *Eur. J. Immunol.* **28**, 257–263 (1998).
17. M. Grell, E. Douni, H. Wajant, M. Lohden, M. Clauss, B. Maxeiner, S. Georgopoulos, W. Lesslauer, G. Kollias, K. Pfizenmaier, P. Scheurich, The transmembrane form of tumor necrosis factor is the prime activating ligand of the 80 kDa tumor necrosis factor receptor. *Cell* **83**, 793–802 (1995).
18. B. M. Saunders, S. Tran, S. Ruuls, J. D. Sedgwick, H. Briscoe, W. J. Britton, Transmembrane TNF is sufficient to initiate cell migration and granuloma formation and provide acute, but not long-term, control of *Mycobacterium tuberculosis* infection. *J. Immunol.* **174**, 4852–4859 (2005).
19. M. L. Olleros, R. Guler, N. Corazza, D. Vesin, H. P. Eugster, G. Marchal, P. Chavarot, C. Mueller, I. Garcia, Transmembrane TNF induces an efficient cell-mediated immunity and resistance to *Mycobacterium bovis* bacillus Calmette-Guerin infection in the absence of secreted TNF and lymphotoxin-α. *J. Immunol.* **168**, 3394–3401 (2002).
20. X. Chen, M. Baumel, D. N. Mannel, O. M. Howard, J. J. Oppenheim, Interaction of TNF with TNF receptor type 2 promotes expansion and function of mouse $CD4^+CD25^+$ T regulatory cells. *J. Immunol.* **179**, 154–161 (2007).
21. R. E. Kontermann, P. Scheurich, K. Pfizenmaier, Antagonists of TNF action: Clinical experience and new developments. *Expert Opin. Drug Discov.* **4**, 279–292 (2009).
22. G. Kollias, D. Kontoyiannis, Role of TNF/TNFR in autoimmunity: Specific TNF receptor blockade may be advantageous to anti-TNF treatments. *Cytokine Growth Factor Rev.* **13**, 315–321 (2002).
23. D. W. Banner, A. D'Arcy, W. Janes, R. Gentz, H. J. Schoenfeld, C. Broger, H. Loetscher, W. Lesslauer, Crystal structure of the soluble human 55 kd TNF receptor-human TNFβ complex: Implications for TNF receptor activation. *Cell* **73**, 431–445 (1993).
24. E. Y. Jones, D. I. Stuart, N. P. Walker, Structure of tumour necrosis factor. *Nature* **338**, 225–228 (1989).
25. M. J. Eck, S. R. Sprang, The structure of tumor necrosis factor-α at 2.6 Å resolution. Implications for receptor binding. *J. Biol. Chem.* **264**, 17595–17605 (1989).
26. S. S. Cha, B. J. Sung, Y. A. Kim, Y. L. Song, H. J. Kim, S. Kim, M. S. Lee, B. H. Oh, Crystal structure of TRAIL-DR5 complex identifies a critical role of the unique frame insertion in conferring recognition specificity. *J. Biol. Chem.* **275**, 31171–31177 (2000).
27. J. Mongkolsapaya, J. M. Grimes, N. Chen, X. N. Xu, D. I. Stuart, E. Y. Jones, G. R. Screaton, Structure of the TRAIL-DR5 complex reveals mechanisms conferring specificity in apoptotic initiation. *Nat. Struct. Biol.* **6**, 1048–1053 (1999).
28. S. G. Hymowitz, H. W. Christinger, G. Fuh, M. Ultsch, M. O'Connell, R. F. Kelley, A. Ashkenazi, A. M. de Vos, Triggering cell death: The crystal structure of Apo2L/TRAIL in a complex with death receptor 5. *Mol. Cell* **4**, 563–571 (1999).
29. D. M. Compaan, S. G. Hymowitz, The crystal structure of the costimulatory OX40-OX40L complex. *Structure* **14**, 1321–1330 (2006).
30. Z. Yang, A. P. West Jr., P. J. Bjorkman, Crystal structure of TNFα complexed with a poxvirus MHC-related TNF binding protein. *Nat. Struct. Mol. Biol.* **16**, 1189–1191 (2009).
31. M. M. Rahman, A. R. Lucas, G. McFadden, Viral TNF inhibitors as potential therapeutics. *Adv. Exp. Med. Biol.* **666**, 64–77 (2009).
32. R. M. Siegel, J. K. Frederiksen, D. A. Zacharias, F. K. Chan, M. Johnson, D. Lynch, R. Y. Tsien, M. J. Lenardo, Fas preassociation required for apoptosis signaling and dominant inhibition by pathogenic mutations. *Science* **288**, 2354–2357 (2000).
33. F. K. Chan, H. J. Chun, L. Zheng, R. M. Siegel, K. L. Bui, M. J. Lenardo, A domain in TNF receptors that mediates ligand-independent receptor assembly and signaling. *Science* **288**, 2351–2354 (2000).
34. L. M. Sedger, S. R. Osvath, X. M. Xu, G. Li, F. K. Chan, J. W. Barrett, G. McFadden, Poxvirus tumor necrosis factor receptor (TNFR)-like T2 proteins contain a conserved preligand assembly domain that inhibits cellular TNFR1-induced cell death. *J. Virol.* **80**, 9300–9309 (2006).
35. L. Clancy, K. Mruk, K. Archer, M. Woelfel, J. Mongkolsapaya, G. Screaton, M. J. Lenardo, F. K. Chan, Preligand assembly domain-mediated ligand-independent association between TRAIL receptor 4 (TR4) and TR2 regulates TRAIL-induced apoptosis. *Proc. Natl. Acad. Sci. U.S.A.* **102**, 18099–18104 (2005).
36. J. M. Kramer, W. Hanel, F. Shen, N. Isik, J. P. Malone, A. Maitra, W. Sigurdson, D. Swart, J. Tocker, T. Jin, S. L. Gaffen, Cutting edge: Identification of a pre-ligand assembly domain (PLAD) and ligand binding site in the IL-17 receptor. *J. Immunol.* **179**, 6379–6383 (2007).
37. G. M. Deng, L. Zheng, F. K. Chan, M. Lenardo, Amelioration of inflammatory arthritis by targeting the pre-ligand assembly domain of tumor necrosis factor receptors. *Nat. Med.* **11**, 1066–1072 (2005).

38. Y. Mukai, T. Nakamura, Y. Yoshioka, S. Tsunoda, H. Kamada, S. Nakagawa, Y. Yamagata, Y. Tsutsumi, Crystallization and preliminary x-ray analysis of the tumour necrosis factor α-tumour necrosis factor receptor type 2 complex. *Acta Crystallogr. Sect. F Struct. Biol. Cryst. Commun.* **65**, 295–298 (2009).
39. H. Shibata, Y. Yoshioka, A. Ohkawa, K. Minowa, Y. Mukai, Y. Abe, M. Taniai, T. Nomura, H. Kayamuro, H. Nabeshi, T. Sugita, S. Imai, K. Nagano, T. Yoshikawa, T. Fujita, S. Nakagawa, A. Yamamoto, T. Ohta, T. Hayakawa, T. Mayumi, P. Vandenabeele, B. B. Aggarwal, T. Nakamura, Y. Yamagata, S. Tsunoda, H. Kamada, Y. Tsutsumi, Creation and x-ray structure analysis of the tumor necrosis factor receptor-1-selective mutant of a tumor necrosis factor-α antagonist. *J. Biol. Chem.* **283**, 998–1007 (2008).
40. Y. Yamamoto, Y. Tsutsumi, Y. Yoshioka, T. Nishibata, K. Kobayashi, T. Okamoto, Y. Mukai, T. Shimizu, S. Nakagawa, S. Nagata, T. Mayumi, Site-specific PEGylation of a lysine-deficient TNF-α with full bioactivity. *Nat. Biotechnol.* **21**, 546–552 (2003).
41. E. Oregon-Romero, M. Vazquez-Del Mercado, R. E. Navarro-Hernandez, N. Torres-Carrillo, G. Martinez-Bonilla, I. Estrada-Garcia, H. Rangel-Villalobos, J. F. Munoz-Valle, Tumor necrosis factor receptor 2 M196R polymorphism in rheumatoid arthritis and osteoarthritis: Relationship with sTNFR2 levels and clinical features. *Rheumatol. Int.* **27**, 53–59 (2006).
42. C. Morita, T. Horiuchi, H. Tsukamoto, N. Hatta, Y. Kikuchi, Y. Arinobu, T. Otsuka, T. Sawabe, S. Harashima, K. Nagasawa, Y. Niho, Association of tumor necrosis factor receptor type II polymorphism 196R with systemic lupus erythematosus in the Japanese: Molecular and functional analysis. *Arthritis Rheum.* **44**, 2819–2827 (2001).
43. N. Tsuchiya, T. Komata, M. Matsushita, J. Ohashi, K. Tokunaga, New single nucleotide polymorphisms in the coding region of human TNFR2: Association with systemic lupus erythematosus. *Genes Immun.* **1**, 501–503 (2000).
44. J. H. Naismith, S. R. Sprang, Modularity in the TNF-receptor family. *Trends Biochem. Sci.* **23**, 74–79 (1998).
45. S. C. Graham, M. W. Bahar, N. G. Abrescia, G. L. Smith, D. I. Stuart, J. M. Grimes, Structure of CrmE, a virus-encoded tumour necrosis factor receptor. *J. Mol. Biol.* **372**, 660–671 (2007).
46. Y. Mukai, H. Shibata, T. Nakamura, Y. Yoshioka, Y. Abe, T. Nomura, M. Taniai, T. Ohta, S. Ikemizu, S. Nakagawa, S. Tsunoda, H. Kamada, Y. Yamagata, Y. Tsutsumi, Structure–function relationship of tumor necrosis factor (TNF) and its receptor interaction based on 3D structural analysis of a fully active TNFR1-selective TNF mutant. *J. Mol. Biol.* **385**, 1221–1229 (2009).
47. C. Reed, Z. Q. Fu, J. Wu, Y. N. Xue, R. W. Harrison, M. J. Chen, I. T. Weber, Crystal structure of TNF-α mutant R31D with greater affinity for receptor R1 compared with R2. *Protein Eng.* **10**, 1101–1107 (1997).
48. X. Van Ostade, J. Tavernier, W. Fiers, Structure-activity studies of human tumour necrosis factors. *Protein Eng.* **7**, 5–22 (1994).
49. H. Loetscher, D. Stueber, D. Banner, F. Mackay, W. Lesslauer, Human tumor necrosis factor α (TNF α) mutants with exclusive specificity for the 55-kDa or 75-kDa TNF receptors. *J. Biol. Chem.* **268**, 26350–26357 (1993).
50. Y. Mukai, T. Nakamura, Y. Yoshioka, H. Shibata, Y. Abe, T. Nomura, M. Taniai, T. Ohta, S. Nakagawa, S. Tsunoda, H. Kamada, Y. Yamagata, Y. Tsutsumi, Fast binding kinetics and conserved 3D structure underlie the antagonistic activity of mutant TNF: Useful information for designing artificial proteo-antagonists. *J. Biochem.* **146**, 167–172 (2009).
51. H. Shibata, Y. Yoshioka, A. Ohkawa, Y. Abe, T. Nomura, Y. Mukai, S. Nakagawa, M. Taniai, T. Ohta, T. Mayumi, H. Kamada, S. Tsunoda, Y. Tsutsumi, The therapeutic effect of TNFR1-selective antagonistic mutant TNF-α in murine hepatitis models. *Cytokine* **44**, 229–233 (2008).
52. W. L. DeLano, M. H. Ultsch, A. M. de Vos, J. A. Wells, Convergent solutions to binding at a protein-protein interface. *Science* **287**, 1279–1283 (2000).
53. P. M. Steed, M. G. Tansey, J. Zalevsky, E. A. Zhukovsky, J. R. Desjarlais, D. E. Szymkowski, C. Abbott, D. Carmichael, C. Chan, L. Cherry, P. Cheung, A. J. Chirino, H. H. Chung, S. K. Doberstein, A. Eivazi, A. V. Filikov, S. X. Gao, R. S. Hubert, M. Hwang, L. Hyun, S. Kashi, A. Kim, E. Kim, J. Kung, S. P. Martinez, U. S. Muchhal, D. H. Nguyen, C. O'Brien, D. O'Keefe, K. Singer, O. Vafa, J. Vielmetter, S. C. Yoder, B. I. Dahiyat, Inactivation of TNF signaling by rationally designed dominant-negative TNF variants. *Science* **301**, 1895–1898 (2003).
54. J. H. Naismith, T. Q. Devine, B. J. Brandhuber, S. R. Sprang, Crystallographic evidence for dimerization of unliganded tumor necrosis factor receptor. *J. Biol. Chem.* **270**, 13303–13307 (1995).
55. J. H. Naismith, T. Q. Devine, T. Kohno, S. R. Sprang, Structures of the extracellular domain of the type I tumor necrosis factor receptor. *Structure* **4**, 1251–1262 (1996).
56. F. K. Chan, Three is better than one: Pre-ligand receptor assembly in the regulation of TNF receptor signaling. *Cytokine* **37**, 101–107 (2007).
57. Y. C. Park, V. Burkitt, A. R. Villa, L. Tong, H. Wu, Structural basis for self-association and receptor recognition of human TRAF2. *Nature* **398**, 533–538 (1999).
58. Q. Yin, S. C. Lin, B. Lamothe, M. Lu, Y. C. Lo, G. Hura, L. Zheng, R. L. Rich, A. D. Campos, D. G. Myszka, M. J. Lenardo, B. G. Darnay, H. Wu, E2 interaction and dimerization in the crystal structure of TRAF6. *Nat. Struct. Mol. Biol.* **16**, 658–666 (2009).
59. Z. Otwinowski, W. Minor, Processing of x-ray diffraction data collected in oscillation mode. *Methods Enzymol.* **276**, 307–326 (1997).
60. A. Vagin, A. Teplyakov, MOLREP: An automated program for molecular replacement. *J. Appl. Crystallogr.* **30**, 1022–1025 (1997).
61. E. Potterton, P. Briggs, M. Turkenburg, E. Dodson, A graphical user interface to the CCP4 program suite. *Acta Crystallogr. D Biol. Crystallogr.* **59**, 1131–1137 (2003).
62. A. T. Brünger, P. D. Adams, G. M. Clore, W. L. DeLano, P. Gros, R. W. Grosse-Kunstleve, J. S. Jiang, J. Kuszewski, M. Nilges, N. S. Pannu, R. J. Read, L. M. Rice, T. Simonson, G. L. Warren, Crystallography & NMR system: A new software suite for macromolecular structure determination. *Acta Crystallogr. D Biol. Crystallogr.* **54**, 905–921 (1998).
63. P. Emsley, K. Cowtan, Coot: Model-building tools for molecular graphics. *Acta Crystallogr. D Biol. Crystallogr.* **60**, 2126–2132 (2004).
64. P. D. Adams, R. W. Grosse-Kunstleve, L. W. Hung, T. R. Ioerger, A. J. McCoy, N. W. Moriarty, R. J. Read, J. C. Sacchettini, N. K. Sauter, T. C. Terwilliger, PHENIX: Building new software for automated crystallographic structure determination. *Acta Crystallogr. D Biol. Crystallogr.* **58**, 1948–1954 (2002).
65. S. C. Lovell, I. W. Davis, W. B. Arendall III, P. I. de Bakker, J. M. Word, M. G. Prisant, J. S. Richardson, D. C. Richardson, Structure validation by Cα geometry: φ,ψ and Cβ deviation. *Proteins* **50**, 437–450 (2003).
66. W. L. DeLano, *The PyMOL Molecular Graphics System* (DeLano Scientific, San Carlos, CA, 2002), http://www.pymol.org.
67. E. Krissinel, K. Henrick, Secondary-structure matching (SSM), a new tool for fast protein structure alignment in three dimensions. *Acta Crystallogr. D Biol. Crystallogr.* **60**, 2256–2268 (2004).
68. J. D. Thompson, D. G. Higgins, T. J. Gibson, CLUSTAL W: Improving the sensitivity of progressive multiple sequence alignment through sequence weighting, position-specific gap penalties and weight matrix choice. *Nucleic Acids Res.* **22**, 4673–4680 (1994).
69. A. Nicholls, K. A. Sharp, B. Honig, Protein folding and association: Insights from the interfacial and thermodynamic properties of hydrocarbons. *Proteins* **11**, 281–296 (1991).

70. **Acknowledgments:** We thank T. Mayumi for his advice about this research. **Funding:** This study was supported in part by Grants-in-Aid for Scientific Research from the Ministry of Education, Culture, Sports, Science and Technology of Japan and from the Japan Society for the Promotion of Science. This study was also supported in part by Health Labour Sciences Research Grants from the Ministry of Health, Labor and Welfare of Japan; Health Sciences Research Grants for Research on Publicly Essential Drugs and Medical Devices from the Japan Health Sciences Foundation; and The Nagai Foundation Tokyo. **Author contributions:** Y.M., S.T., and Y.T. designed the research; Y.M., T.N., and M.Y. performed the research; Y.M., T.N., and Y. Yamagata analyzed the data; Y. Yoshioka and S.N. contributed new reagents; and Y.M., Y. Yamagata, and Y.T. wrote the paper. **Competing interests:** The authors declare that they have no competing interests. **Accession numbers:** Coordinates and structure factors have been deposited in the PDB with the accession number 3alq.

Submitted 24 February 2010
Accepted 29 October 2010
Final Publication 16 November 2010
10.1126/scisignal.2000954
Citation: Y. Mukai, T. Nakamura, M. Yoshikawa, Y. Yoshioka, S.-i. Tsunoda, S. Nakagawa, Y. Yamagata, Y. Tsutsumi, Solution of the structure of the TNF-TNFR2 complex. *Sci. Signal.* **3**, ra83 (2010).

International Immunopharmacology 10 (2010) 26–33

Contents lists available at ScienceDirect

International Immunopharmacology

journal homepage: www.elsevier.com/locate/intimp

Comparison of the anti-tumor activity of native, secreted, and membrane-bound LIGHT in mouse tumor models

Tomohiro Morishige [a,1], Yasuo Yoshioka [a,b,*,1], Aya Tanabe [a], Xinglei Yao [a], Hiroyuki Mizuguchi [c,d], Shin-ichi Tsunoda [e], Yasuo Tsutsumi [e,f], Yohei Mukai [a], Naoki Okada [a], Shinsaku Nakagawa [a,b]

[a] Laboratory of Biotechnology and Therapeutics, Graduate School of Pharmaceutical Sciences, Osaka University, Japan
[b] The Center for Advanced Medical Engineering and Informatics, Osaka University, Japan
[c] Laboratory of Biochemistry and Molecular Biology, Graduate School of Pharmaceutical Sciences, Osaka University, Japan
[d] Laboratory of Gene Transfer and Regulation, National Institute of Biomedical Innovation, Japan
[e] Laboratory of Pharmaceutical Sciences, National Institute of Biomedical Innovation, Japan
[f] Laboratory of Toxicology, Graduate School of Pharmaceutical Sciences, Osaka University, Japan

ARTICLE INFO

Article history:
Received 10 March 2009
Received in revised form 21 September 2009
Accepted 23 September 2009

Keywords:
Adenovirus vector
Cancer gene therapy
Cytokine
LIGHT
Lymphotoxin

ABSTRACT

The TNF superfamily member LIGHT has potent anti-tumor activity through direct cytotoxicity and activation of the immune response, and is a promising candidate for cancer therapy. Natively, LIGHT exists as both a membrane-anchored form and a proteolytically processed, secreted form. However, the strength of the anti-tumor activity of each form of LIGHT has not been well defined. Here, to identify the optimal form of LIGHT for cancer gene therapy, we constructed fiber-mutant adenovirus vectors (AdRGD) encoding native full-length LIGHT (LIGHT/FL), stably membrane-anchored LIGHT (LIGHT/mem), and fully secreted LIGHT (LIGHT/sec). We then compared the anti-tumor effects of the different forms of LIGHT in mice by intratumoral injection of each AdRGD. We demonstrated that intratumoral injection of AdRGD-LIGHT/sec provided greater tumor suppression than AdRGD-LIGHT/FL, although this effect did not reach statistical significance. By comparison, AdRGD-LIGHT/mem had negligible anti-tumor activity. We also demonstrated that more CD4+ and CD8+ T cells accumulated inside tumors treated *in vivo* with AdRGD-LIGHT/sec than in tumors treated with AdRGD-LIGHT/FL or AdRGD-LIGHT/mem. These results suggest that the secreted form of LIGHT might be the optimal form for cancer gene therapy.

1. Introduction

The tumor necrosis factor (TNF) superfamily member LIGHT, whose name is derived from and homologous to lymphotoxins, shows inducible expression, and competes with herpes simplex virus (HSV) glycoprotein D for the herpesvirus entry mediator (HVEM), a receptor expressed by T lymphocytes, is a 29-kDa type II transmembrane protein produced by activated T cells, monocytes, granulocytes, and immature dendritic cells (DCs) [1]. LIGHT functions as a ligand for two functional TNF family receptors, the lymphotoxin β receptor (LTβR), expressed on epithelial and stromal cells but conspicuously absent from lymphocytes, and the HVEM, expressed predominately in T cells [2,3]. The LTβR signaling pathway plays a crucial role in ectopic lymphoid organogenesis, a key process in the induction of the immune response [4]. In cancer treatment, the engagement of LIGHT with LTβR triggers apoptosis of some human cancer cells and promotes cytokine production and the release of the naive T-cell attractant chemokine CCL21 in stromal cells [5–7]. LIGHT-HVEM signaling functions as a co-stimulatory molecule for T-cell activation [2,8,9]. In addition, the engagement of LIGHT with HVEM stimulates T-cell proliferation and IFN-γ secretion [2,8].

The forced expression of LIGHT in neoplastic cells induces the rejection of an established tumor by increasing lymphocytic infiltration, tumor necrosis, and T-cell cytotoxic activity [10]. Furthermore, Yu et al. reported that the local delivery of the LIGHT gene into the primary tumor not only prevents growth of the established tumor, but also eradicates established metastases in peripheral tissues by the activation and augmentation of tumor immunity via LTβR and HVEM [6,11]. Taken together, these findings show that the constitutive expression of LIGHT within a tumor can regulate anti-tumor T-cell-mediated immunity and highlight LIGHT as a promising candidate for cancer gene therapy.

The extracellular domains of many membrane proteins can be proteolytically cleaved. This proteolytic processing, also referred to as ectodomain shedding, is observed in cytokines, receptors of cytokines, and other membrane proteins [12–15]. The ectodomain shedding of membrane proteins changes their fate, location, and mode of action. Differences in the biological activity between secreted and membrane-anchored forms have been described for members of the TNF ligand

* Corresponding author. The Center for Advanced Medical Engineering and Informatics, Osaka University, 1-6, Yamadaoka, Suita, Osaka, 565-0871, Japan. Tel./fax: +81 6 6879 8177.
E-mail address: yasuo@phs.osaka-u.ac.jp (Y. Yoshioka).
[1] Each author contributed equally to the work.

1567-5769/$ – see front matter © 2009 Elsevier B.V. All rights reserved.
doi:10.1016/j.intimp.2009.09.014

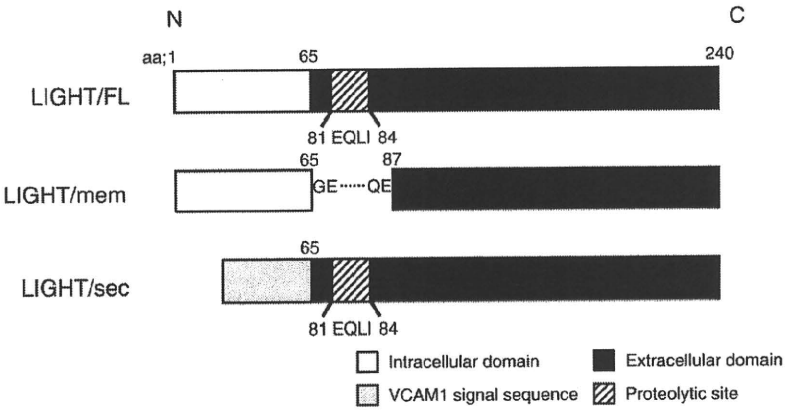

Fig. 1. Schematic representation of LIGHT/FL, LIGHT/mem, and LIGHT/sec. LIGHT/mem; amino acids 66 to 86, including the proteolytic site, were deleted from full-length LIGHT to ensure stable surface expression by tumor cells. LIGHT/sec; extracellular domain of LIGHT, amino acids 66 to 240, was fused to the C-terminus of the VCAM1 signal peptide.

superfamily, for example Fas ligand (FasL) and TNF-α [12,13]. Gregory et al. reported a marked difference in the anti-tumor effect between secreted FasL and membrane-anchored FasL in tumor cells constitutively expressing these proteins [16]. Similar to FasL, native LIGHT also exists as a membrane-anchored form and is proteolytically cleaved from the membrane by matrix metalloproteinases (MMP) to produce the mature, secreted, 25-kDa form [6,17,18]. Differences in the function and anti-tumor activity of native full-length LIGHT (LIGHT/FL), stably membrane-anchored LIGHT (LIGHT/mem), and fully secreted LIGHT (LIGHT/sec), remain unknown, but understanding these differences is necessary to identify the optimal form of LIGHT for cancer gene therapy.

Here, we investigated the differences in anti-tumor activity between native, secreted and membrane-anchored LIGHT. First, we constructed Arg-Gly-Asp (RGD) fiber-mutant adenovirus (Ad) vectors (AdRGD), which efficiently transfer foreign genes into target cells, including tumor cells, to express LIGHT/FL, LIGHT/mem, or LIGHT/sec. Then, we compared the anti-tumor effects of the different forms of LIGHT *in vivo* by intratumoral injection of each AdRGD.

2. Materials and methods

2.1. Cells and animals

HT29.14S cells, which are clones of the HT29 colon adenocarcinoma cell line, were kindly provided by Dr. CF Ware (La Jolla Institute for Allergy and Immunology, CA) and cultured in DMEM supplemented with 10% FBS and antibiotics. Murine colon carcinoma CT26 cells were kindly provided by Dr. NP Restifo (National Cancer Institute, Bethesda, MD), cultured in RPMI 1640 medium supplemented with 10% FBS and antibiotics. Murine melanoma B16BL6 cells were purchased from the JCRB cell bank (Tokyo, Japan) and cultured in MEM supplemented with 7.5% FBS and antibiotics. Female BALB/c mice and C57BL/6 mice were purchased from Nippon SLC (Kyoto, Japan) and used at 6 to 8 weeks of age. All of the animal experimental procedures in this study were performed in accordance with the Osaka University guidelines for the welfare of animals.

2.2. Construction of Ads

Human LIGHT cDNA was kindly provided by Dr. K Tamada (University of Maryland, Baltimore, MD). We used full-length human LIGHT sequence as a template to generate DNA fragments by PCR: fragment-LIGHT/FL, fragment-LIGHT/mem, and fragment-LIGHT/sec. For fragment-LIGHT/FL, sense primer 5′-CGTCTAGAATGGAGGAGAGTGTCGTACGG CCCTC-3′ and antisense primer 5′-ATGCGGCCGC TCATCACACC ATGAAAGCCC CGAAG-3′ were used; for fragment-LIGHT/mem, sense primer 5′-CTCCCTGCAGCT GCACTGGCGTCTACGAAGGTCTCACGAGGTCAACCCAG-3′ and the antisense primer described above were used; for fragment-LIGHT/sec, sense primer 5′-CGTCTAGAATGCCTGGGAAGATGGTCGTGATCCTTGGAGCCT-CAAATATACTTTGGATAATGTTTGCAGCTTCTCAAGCTGGAGAGATGGT-CACCCGCCTGCC-3′ and the antisense primer described above were used. The resultant products were cloned into pHM-CMV5. Then AdRGD-LIGHTs that carried the various forms of the human LIGHT gene were constructed by an improved *in vitro* ligation method [19,20]. Each Ad was generated by established methods [19]. Luciferase-expressing AdRGD (AdRGD-Luc) was previously constructed [21]. The virus particles and biological titer (infectious unit; IFU) were determined by a spectrophotometrical method and by using an Adeno-X Rapid Titer protocol (Clontech Laboratories, Mountain View, CA, USA), respectively [22]. The particle-to-biological titer ratio was between 10 and 40 for each Ad used in this study.

2.3. Evaluation of production levels of LIGHT from transduced cells in vitro

HT29.14S and B16BL6 cells were transduced with each Ad for 2 h at 500 IFU/cell. The cells were washed and cultured for another 22 h in media containing 10% FBS. The supernatants were collected, and the level of LIGHT for each Ad was measured with the Human LIGHT Enzyme Immunosorbent Assay Kit (R&D Systems, Minneapolis, MN). The expression level of LIGHT on the cell surface was assessed with the anti-human LIGHT/TNFSF14 monoclonal antibody (R&D systems) and a FITC-conjugated rat anti-mouse Igκ light chain monoclonal antibody (BD Pharmingen, San Diego, CA) by flow cytometry on a FACSCalibur flow cytometer.

2.4. Cytotoxicity assay

HT29.14S cells (5000 cells/well) were incubated for 12 h at 37 °C. Then cells were transduced with AdRGDs at 10, 100, or 500 IFU/cell in the presence of 10 units/mL human IFN-γ. After 56 h, cell viability was assessed by the WST-8 assay according to the manufacturer's instructions. The OD450-650 was measured with a multiwell spectrophotometer (Spectra Max M5Y, Molecular Devices, Inc.).

2.5. Animal studies

C57BL/6 mice or BALB/c mice were intradermally inoculated with 2×10^5 cells (B16BL6) or 5×10^5 cells (CT26), respectively, into the flank. Seven days later, established tumors with diameters of 5–7 mm were treated with each Ad at 5×10^8 (B16BL6) or 7×10^7 (CT26) IFU in 50 μL PBS, respectively. Tumor size was measured with calipers 3 times a week, and tumor volume was calculated using the following

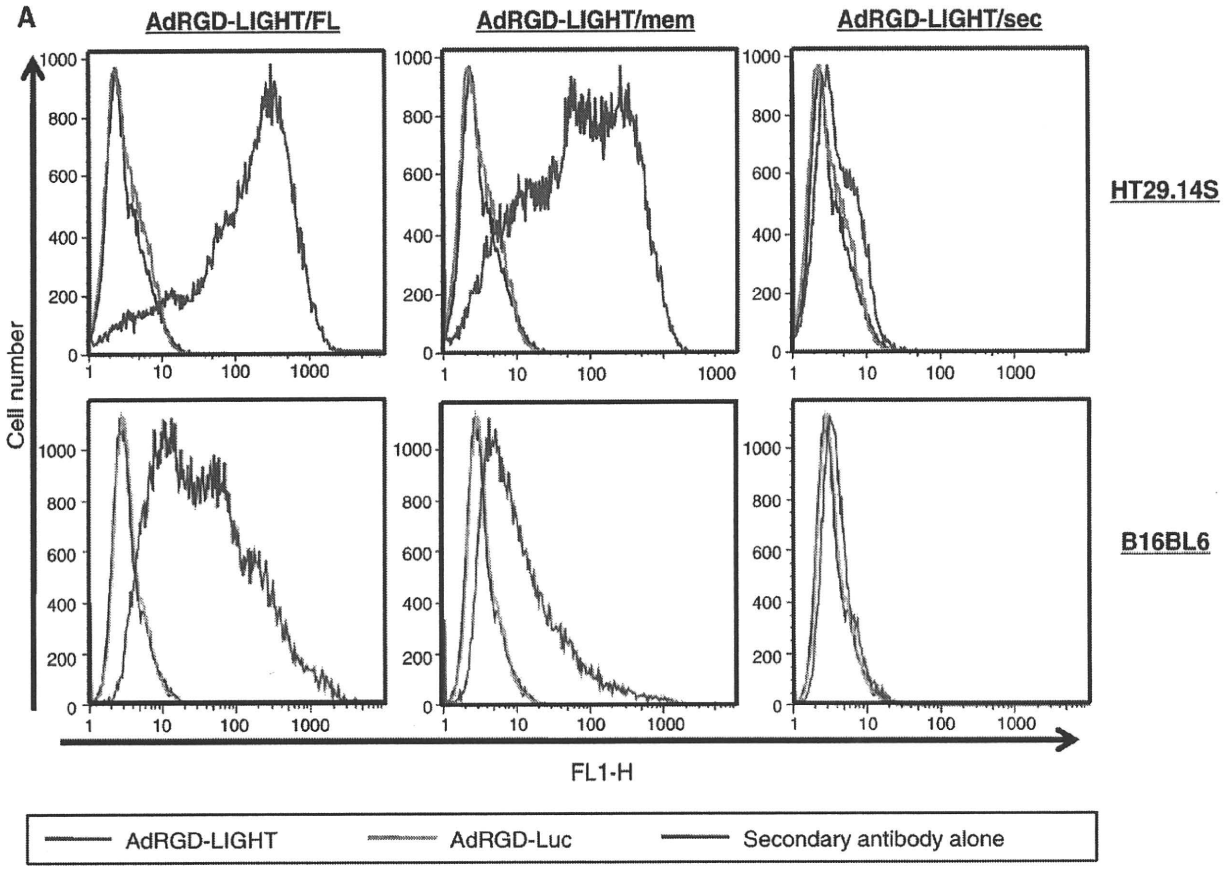
A
AdRGD-LIGHT/FL
AdRGD-LIGHT/mem
AdRGD-LIGHT/sec
HT29.14S
B16BL6
Cell number
FL1-H
AdRGD-LIGHT
AdRGD-Luc
Secondary antibody alone

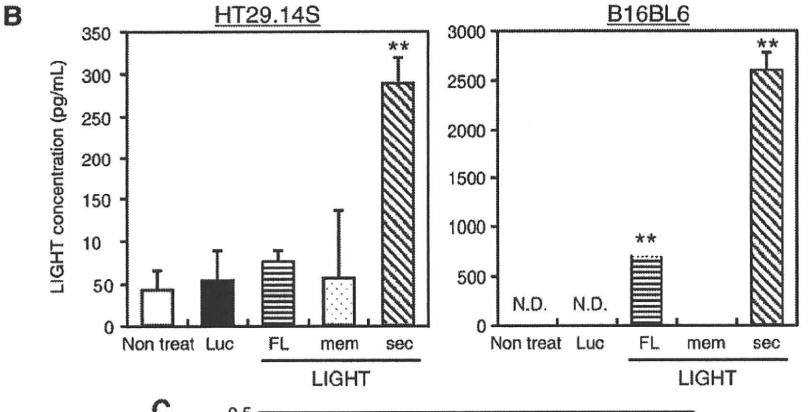
B
HT29.14S
B16BL6
LIGHT concentration (pg/mL)
N.D.
Non treat
Luc
FL
mem
sec
LIGHT

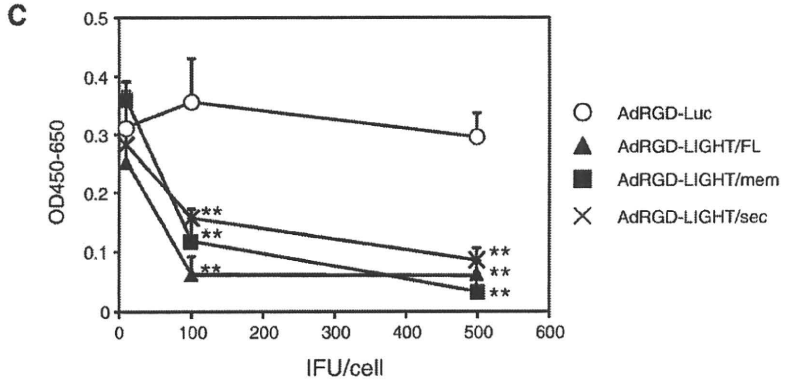
C
OD450-650
IFU/cell
AdRGD-Luc
AdRGD-LIGHT/FL
AdRGD-LIGHT/mem
AdRGD-LIGHT/sec

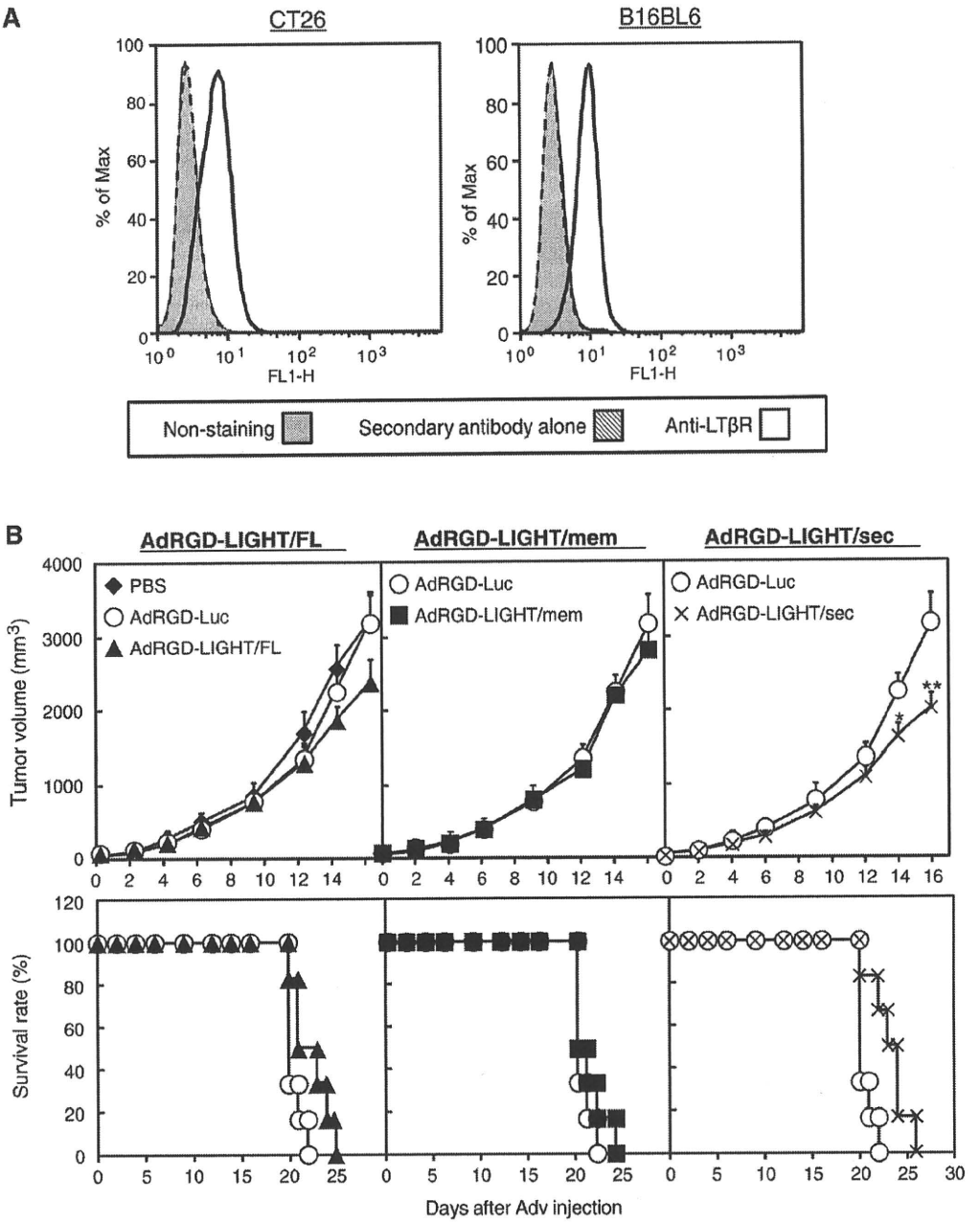

Fig. 3. Therapeutic effect of intratumorally injected AdRGD-LIGHTs. (A) LTβR expression in CT26 and B16BL6 cells. LTβR expression on the cell surface of CT26 and B16BL6 cells was determined by flow cytometry analysis using the anti-LTβR antibody. The open curve shows staining with the anti-mouse LTβR antibody. The filled and slashed curves show non-staining and the secondary antibody only control. (B) B16BL6 cells (2×10^5 cells/mouse) or (C) CT26 cells (5×10^5 cells/mouse) were intradermally inoculated into C57BL/6 or BALB/c mice, respectively. Seven days later, the tumors were treated with the AdRGD-LIGHTs. The tumor volume and prolonged survival time of tumor-bearing mice were monitored. Data were calculated according to the formula described in Section 2, and each point represents the mean ± SEM for six mice. (* $P<0.05$ and ** $P<0.01$ compared with AdRGD-Luc by the Student's *t*-test.).

formula: (tumor volume; mm^3) = (major axis; mm) × (minor axis; $mm)^2\times0.5$. Mice bearing tumors with a major axis greater than 25 mm were euthanized. All animal experiments were carried out in accordance with protocols approved by the Animal Care and Use Committee of the Graduate School of Pharmaceutical Sciences, Osaka University, Japan.

Fig. 2. Confirmation of the form and biological activity of LIGHT. (A) Flow cytometric analysis of LIGHT expression. HT29.14S and B16BL6 cells were transduced with AdRGD-LIGHTs at the dose of 500 IFU/cell. The expression of LIGHT on the cell surface was detected by flow cytometric analysis. The blue curve shows staining with the anti-human LIGHT antibody. (B) Quantification of the secreted soluble form of LIGHT by ELISA. HT29.14S and B16BL6 cells were transduced with AdRGD-LIGHTs at the dose of 500 IFU/cell. LIGHT concentration in the culture supernatant was measured by ELISA. Each point represents the mean ± SD. (** $P<0.01$ versus value for AdRGD-Luc by ANOVA.) (C) Confirmation of biological activity of LIGHT expressed by each AdRGD. HT29.14S cells were transduced with AdRGD-LIGHTs in the presence of 10 units/mL of human IFN-γ. These transduced cells were incubated for 56 h. Cytotoxicity was evaluated by the WST-8 assay. Each point represents the mean ± SD. (** $P<0.01$ versus value for AdRGD-Luc by ANOVA.).

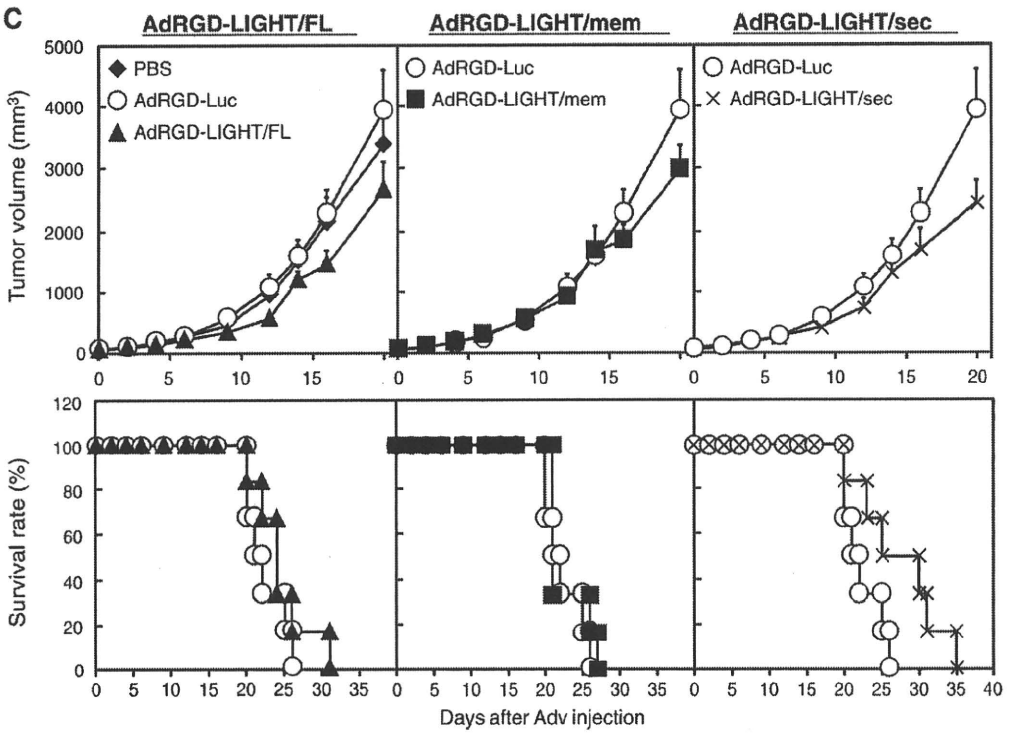

Fig. 3 (*continued*).

2.6. Detection of CD4+ and CD8+ T cells in tumors

BALB/c mice were intradermally inoculated with 5×10^5 CT26 cells into the flank. Seven days later, established tumors with diameters of 5–7 mm were treated with each Ad at 7×10^7 IFU. Eighteen days after intratumoral injection with Ads, CT26 tumors were removed, embedded in OCT compound (Sakura Finetechnical, Tokyo, Japan), and frozen in liquid nitrogen. Frozen sections (7 μm thick) were fixed in 4% paraformaldehyde at 4 °C for 10 min and treated with a primary anti-mouse CD4 or anti-mouse CD8 antibody (BD Pharmingen) at room temperature for 2 h. After washes, the sections were stained with the secondary antibody conjugated with Alexa Fluor 594 Anti-Rat IgG (Molecular Probes) at room temperature for 2 h. Then, the frozen sections were mounted with Prolong Gold with DAPI (Invitrogen, Carlsbad, CA) for nuclear staining, and then photographed with a fluorescence microscope (BZ-8000; Keyence Corporation, Osaka, Japan). Quantification of CD4+ and CD8+ cells in the frozen sections was performed by counting the number of cells in four random high-power fields.

2.7. Statistical analysis

All results are expressed as means ± SEM or SD. Differences were compared by using the Student's *t*-test or Scheffe's method after analysis of variance (ANOVA).

3. Results

3.1. Construction of Ad vectors encoding various forms of LIGHT

We used the AdRGD system, which exhibits α_v-integrin tropism due to an RGD peptide inserted into the HI loop of the fiber knob, to achieve high levels of LIGHT gene expression. This vector system has superior gene transduction efficiency of cancer cells *in vitro* and *in vivo* compared with the conventional Ad vectors [21,23]. We constructed AdRGD encoding LIGHT/FL, which is sensitive to ectodomain shedding creating both secreted and membrane-anchored forms of LIGHT. We also constructed AdRGD encoding only LIGHT/mem, which lacks amino acids from Gly66 to Glu86, including the key proteolytic site (amino acid Glu81-Ile84), and AdRGD encoding only LIGHT/sec, which consists of an extracellular domain of LIGHT composed of amino acids Gly66 to Val240 linked to a signal peptide from VCAM1 to direct secretion (Fig. 1).

3.2. Confirmation of biological activity of various forms of LIGHT

To confirm that each AdRGD-LIGHT constructed here expressed the LIGHT protein in the intended form, we examined the expression patterns of LIGHT on the surface or in the culture supernatant of cells transduced with each AdRGD. First, we analyzed the expression of the LIGHT protein on the surface of HT29.14S or B16BL6 cells by flow cytometry. We detected LIGHT on the surface of HT29.14S and B16BL6 cells transduced with AdRGD-LIGHT/FL and AdRGD-LIGHT/mem, but not on the surface of those transduced with AdRGD-LIGHT/sec or the AdRGD-Luc control (Fig. 2A). Then, to confirm the expression of the secreted form of LIGHT, we quantified the levels of the LIGHT protein in the culture supernatant of transduced HT29.14S and B16BL6 cells by ELISA. We found that for HT29.14S and B16BL6 cells, AdRGD-LIGHT/sec secreted higher levels of LIGHT than AdRGD-LIGHT/FL or AdRGD-LIGHT/mem (Fig. 2B). For B16BL6 cells transduced with AdRGD-LIGHT/FL, we also detected secreted LIGHT in the culture supernatant. This is probably the result of cleavage of full-length LIGHT expressed on the cellular surface by MMP produced by B16BL6 cells. On the other hand, we did not detect LIGHT in the culture supernatant of cells transduced with AdRGD-LIGHT/mem or AdRGD-Luc control. Taken together, these results show that each AdRGD-LIGHT expressed the intended form of LIGHT protein, at least when transfected into B16BL6 cells. By comparison, we could not detect LIGHT in the culture supernatant of HT29.14S cells transfected with AdRGD-LIGHT/FL. We consider that this is probably because HT29.14S cells do not express MMPs.

Next, to examine whether the LIGHT proteins expressed by each AdRGD-LIGHT were biologically active, we transduced HT29.14S cells, which are sensitive to the proapoptotic effect of LIGHT, with the AdRGD-

LIGHTs in the presence of 10 units/mL of human IFN-γ (Fig. 2C) [5,24]. We found that the viability of HT29.14S cells transduced with each AdRGD-LIGHT was significantly lower than the viability of cells transduced with the control vector AdRGD-Luc and was dependent upon vector dose. These results indicate that AdRGD-LIGHTs constructed here express LIGHT with sustained activity.

3.3. Therapeutic effect of intratumorally injected AdRGD-LIGHTs

To assess the therapeutic potential of the AdRGD-LIGHTs, we evaluated the anti-tumor effect of a single intratumoral injection of each AdRGD-LIGHT in mice bearing established B16BL6 and CT26 tumors [25,26]. The expression of LTβR by B16BL6 cells and CT26 cells was confirmed by flow cytometric analysis (Fig. 3A). In both Bl6BL6 and CT26 tumors, tumor growth in mice treated with AdRGD-Luc was comparable to that of PBS-treated mice (Fig. 3B, C). In the B16BL6 tumor model, AdRGD-LIGHT/FL and AdRGD-LIGHT/sec showed tumor-suppressing effects, whereas AdRGD-LIGHT/mem did not (Fig. 3B). Furthermore, AdRGD-LIGHT/sec had a stronger tumor-suppressing effect than AdRGD-LIGHT/FL. In the CT26 tumor model, AdRGD-LIGHT/sec provided the strongest tumor-suppressing effect of all the AdRGD-LIGHTs and tended to prolong the survival more than the AdRGD-Luc

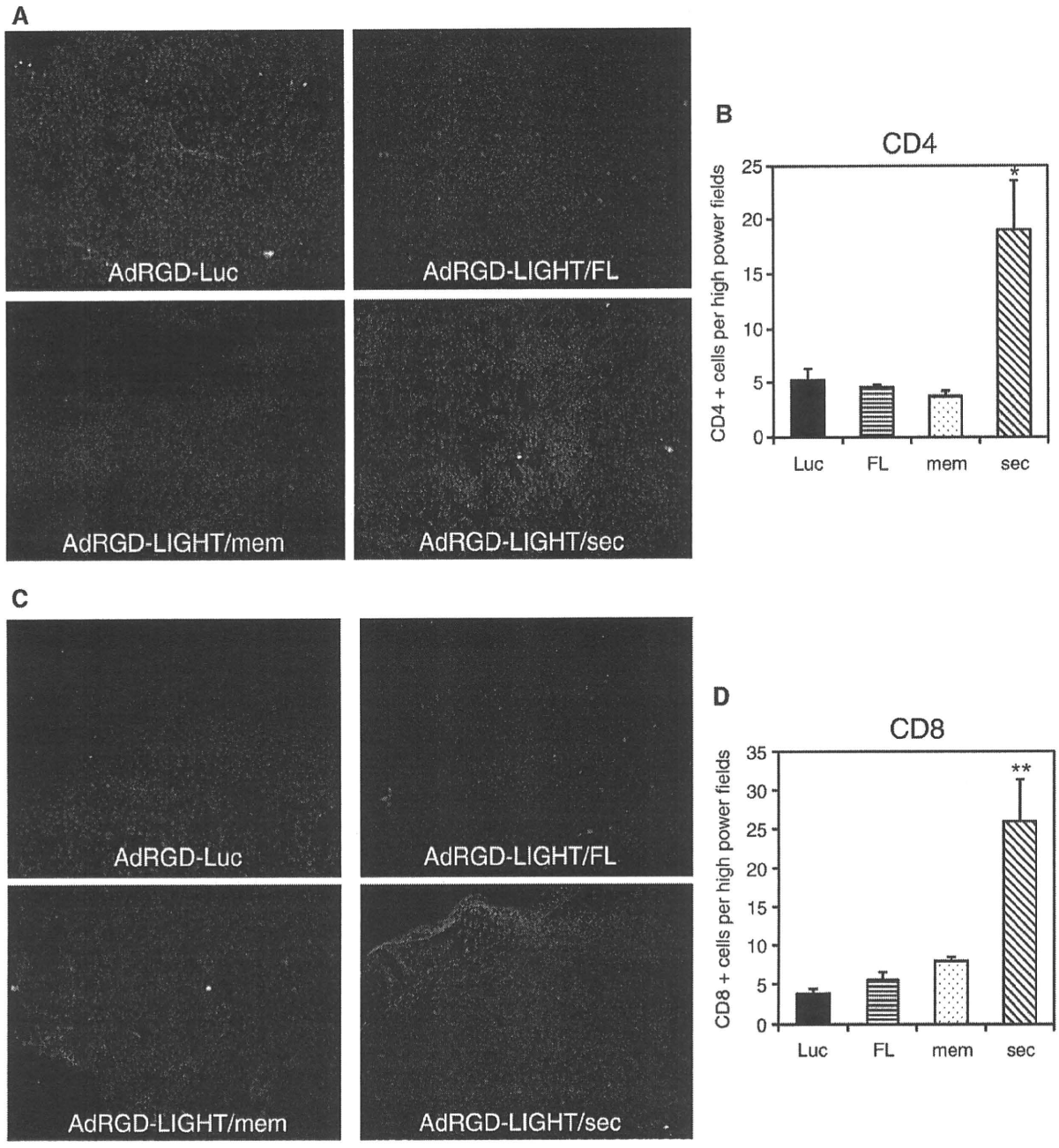

Fig. 4. Histological analysis of tumors administered each AdRGD-LIGHT. CT26 cells (5×10^5 cells/mouse) were intradermally inoculated into BALB/c mice. Seven days later, the tumors were intratumorally treated with each AdRGD-LIGHT. Tumor tissues were collected 18 days after injection and were then embedded in OCT compound and frozen. (A) Frozen sections of tumor tissues were fixed and stained with an anti-mouse CD4 antibody together with an Alexa Fluor 594-conjugated secondary antibody. (B) Quantification of CD4+ cells. (C) Tumors were similarly stained with an anti-mouse CD8 antibody together with an Alexa Fluor 594-conjugated secondary antibody. (D) Quantification of CD8+ cells. Each bar represents the mean ± SEM of the number of CD4+ or CD8+ cells in four random high-power fields (* $P<0.05$ and ** $P<0.01$ versus value for AdRGD-Luc by ANOVA).

control, but this difference was not significant (Fig. 3C). These data indicate that the rank order of the anti-tumor effect of these 3 forms of LIGHT was LIGHT/sec > LIGHT/FL > LIGHT/mem. In addition, we confirmed that mice treated with the AdRGD-LIGHTs did not lose body weight (data not shown). These results suggest that AdRGD-LIGHT/sec efficiently suppresses tumor growth without severe side effects.

3.4. The mechanism of anti-tumor effects of AdRGD-LIGHT/sec

To investigate the mechanism underlying the anti-tumor effects of AdRGD-LIGHT/sec, we assessed the infiltration of immune cells into the tumor mass following intratumoral administration of each AdRGD-LIGHT (Fig. 4). At 18 days after injection, intradermal tumor nodules were resected from tumor-bearing mice for histological examination. We observed more extensive infiltration of CD4+ (Fig. 4A, B) and CD8+ (Fig. 4C, D) T cells in tumors of mice treated with AdRGD-LIGHT/sec than in those treated with the AdRGD-Luc control. By comparison, there was little or no infiltration of CD4+ and CD8+ cells in tumors of mice treated with AdRGD-LIGHT/FL or LIGHT/mem compared with those treated with the AdRGD-Luc control. These findings suggest that the substantial increase in the number of CD4+ and CD8+ T cells within tumors induced by AdRGD-LIGHT/sec might activate tumor-specific immunity in mice.

4. Discussion

LIGHT is a promising candidate for cancer therapy [10,27,28]. However, the difference in anti-tumor activity between membrane-anchored and secreted LIGHT has not been well defined. Here, we compared the potency of the anti-tumor effect of different forms of LIGHT to identify the optimal form for cancer gene therapy.

It has been reported that, in mouse tumor models, membrane-anchored LIGHT exhibits a potent therapeutic effect against various cancers [6,11]. However, in our therapeutic model, secreted LIGHT exhibited a superior therapeutic effect: a single intratumoral injection of AdRGD-LIGHT/sec gave the most efficient anti-tumor effect of all forms of LIGHT, whereas AdRGD-LIGHT/mem gave negligible tumor suppression. Although the mechanism underlying this phenomenon remains unclear, we confirmed that B16BL6 and CT26 cells were resistant to the proapoptotic effect of LIGHT (data not shown), and therefore in our therapeutic model, the main contributing factor to the tumor-suppressing effect of LIGHT might be the activation of cancer immunity. We hypothesized that secreted LIGHT expressed by AdRGD-LIGHT/sec might be efficiently distributed throughout the tumor mass and could induce cancer immunity over a broad area of the tumor, whereas membrane-anchored LIGHT might be restricted to a limited area near the AdRGD vector injection site. This notion was confirmed by our finding that AdRGD-LIGHT/sec efficiently induced infiltration of CD4+ and CD8+ T cells in the tumor mass, whereas LIGHT/mem failed to do so (Fig. 4). However, we observed only a slight, not dramatic, therapeutic effect of AdRGD-LIGHT/sec. In this study, we used the human LIGHT, which was shown by Shaikh et al. to bind to the mouse LTβR and mouse HVEM with an affinity nearly 10-fold lower than that of mouse LIGHT [29]. Thus, we speculate that the inadequate susceptibility of CT26 and B16BL6 tumors to AdRGD-LIGHT/sec in our therapeutic model is the result of differences between human and mouse LIGHT.

Successful cancer gene therapy requires treatment of not only the primary tumor but also distant metastases, which are the major cause of mortality from cancer. Yu et al. reported that local delivery of the gene encoding LIGHT/mem into the primary tumor prevents the formation of metastases [11]. They showed that the primary tumor becomes a major site for the production of CTL, which eradicates established metastatic tumors. Here, we showed that treatment by AdRGD-LIGHT/sec induces T-cell activation within the tumor mass. Moreover, Lukashev et al. examined the production of LTβR in human tumor tissues and found that 87% to 96% of colorectal, lung, larynx/pharynx, stomach, and melanoma tumors were positive for LTβR [30]. Thus, we speculate that AdRGD-LIGHT/sec might have the potential to restrain metastasis and recrudescence of tumors.

In this study, we compared the anti-tumor potential of various forms of LIGHT expressed by AdRGD-LIGHTs and showed that secreted LIGHT had the strongest anti-tumor activity in mouse models of aggressive and established tumors. These results suggest that the secreted form of LIGHT might be the optimal form for cancer gene therapy.

Acknowledgements

The authors declare no conflict of interests. This study was supported in part by grants from the Ministry of Health, Labor, and Welfare of Japan; by the Research on Health Sciences focusing on Drug Innovation from the Japan Health Sciences Foundation; and by the Takeda Science Foundation.

References

[1] Mauri DN, Ebner R, Montgomery RI, Kochel KD, Cheung TC, et al. LIGHT, a new member of the TNF superfamily, and lymphotoxin alpha are ligands for herpesvirus entry mediator. Immunity 1998;8:21–30.
[2] Harrop JA, McDonnell PC, Brigham-Burke M, Lyn SD, Minton J, Tan KB, et al. Herpesvirus entry mediator ligand (HVEM-L), a novel ligand for HVEM/TR2, stimulates proliferation of T cells and inhibits HT29 cell growth. J Biol Chem 1998;273:27548–56.
[3] Murphy M, Walter BN, Pike-Nobile L, Fanger NA, Guyre PM, Browning JL, et al. Expression of the lymphotoxin beta receptor on follicular stromal cells in human lymphoid tissues. Cell Death Differ 1998;5:497–505.
[4] Wang J, Foster A, Chin R, Yu P, Sun Y, Wang Y, et al. The complementation of lymphotoxin deficiency with LIGHT, a newly discovered TNF family member, for the restoration of secondary lymphoid structure and function. Eur J Immunol 2002;32:1969–79.
[5] Rooney IA, Butrovich KD, Glass AA, Borboroglu S, Benedict CA, Whitbeck JC, et al. The lymphotoxin-beta receptor is necessary and sufficient for LIGHT-mediated apoptosis of tumor cells. J Biol Chem 2000;275:14307–15.
[6] Yu P, Lee Y, Liu W, Chin RK, Wang J, Wang Y, et al. Priming of naive T cells inside tumors leads to eradication of established tumors. Nat Immunol 2004;5:141–9.
[7] Stopfer P, Mannel DN, Hehlgans T. Lymphotoxin-beta receptor activation by activated T cells induces cytokine release from mouse bone marrow-derived mast cells. J Immunol 2004;172:7459–65.
[8] Tamada K, Shimozaki K, Chapoval AI, Zhai Y, Su J, Chen SF, et al. LIGHT, a TNF-like molecule, costimulates T cell proliferation and is required for dendritic cell-mediated allogeneic T cell response. J Immunol 2000;164:4105–10.
[9] Wang J, Lo JC, Foster A, Yu P, Chen HM, Wang Y, et al. The regulation of T cell homeostasis and autoimmunity by T cell-derived LIGHT. J Clin Invest 2001;108:1771–80.
[10] Fan Z, Yu P, Wang Y, Fu ML, Liu W, Sun Y, et al. NK-cell activation by LIGHT triggers tumor-specific CD8+ T-cell immunity to reject established tumors. Blood 2006;107:1342–51.
[11] Yu P, Lee Y, Wang Y, Liu X, Auh S, Gajewski TF, et al. Targeting the primary tumor to generate CTL for the effective eradication of spontaneous metastases. J Immunol 2007;179:1960–8.
[12] Schneider P, Holler N, Bodmer JL, Hahne M, Frei K, Fontana A, et al. Conversion of membrane-bound Fas(CD95) ligand to its soluble form is associated with downregulation of its proapoptotic activity and loss of liver toxicity. J Exp Med 1998;187:1205–13.
[13] Grell M, Douni E, Wajant H, Lohden M, Clauss M, Maxeiner B, et al. The transmembrane form of tumor necrosis factor is the prime activating ligand of the 80 kDa tumor necrosis factor receptor. Cell 1995;83:793–802.
[14] Esch FS, Keim PS, Beattie EC, Blacher RW, Culwell AR, Oltersdorf T, et al. Cleavage of amyloid beta peptide during constitutive processing of its precursor. Science 1990;248:1122–4.
[15] Subramanian SV, Fitzgerald ML, Bernfield M. Regulated shedding of syndecan-1 and -4 ectodomains by thrombin and growth factor receptor activation. J Biol Chem 1997;272:14713–20.
[16] Gregory MS, Saff RR, Marshak-Rothstein A, Ksander BR. Control of ocular tumor growth and metastatic spread by soluble and membrane Fas ligand. Cancer Res 2007;67:11951–8.
[17] Anand S, Wang P, Yoshimura K, Choi IH, Hilliard A, Chen YH, et al. Essential role of TNF family molecule LIGHT as a cytokine in the pathogenesis of hepatitis. J Clin Invest 2006;116:1045–51.
[18] Morel Y, Schiano de Colella JM, Harrop J, Deen KC, Holmes SD, Wattam TA, et al. Reciprocal expression of the TNF family receptor herpes virus entry mediator and its ligand LIGHT on activated T cells: LIGHT down-regulates its own receptor. J Immunol 2000;165:4397–404.
[19] Mizuguchi H, Kay MA. Efficient construction of a recombinant adenovirus vector by an improved in vitro ligation method. Hum Gene Ther 1998;9:2577–83.

[20] Mizuguchi H, Kay MA. A simple method for constructing E1- and E1/E4-deleted recombinant adenoviral vectors. Hum Gene Ther 1999;10:2013–7.
[21] Mizuguchi H, Hayakawa T. Enhanced antitumor effect and reduced vector dissemination with fiber-modified adenovirus vectors expressing herpes simplex virus thymidine kinase. Cancer Gene Ther 2002;9:236–42.
[22] Maizel Jr JV, White DO, Scharff MD. The polypeptides of adenovirus. I. Evidence for multiple protein components in the virion and a comparison of types 2, 7A, and 12. Virology 1968;36:115–25.
[23] Okada Y, Okada N, Mizuguchi H, Takahashi K, Hayakawa T, Mayumi T, et al. Optimization of antitumor efficacy and safety of in vivo cytokine gene therapy using RGD fiber-mutant adenovirus vector for preexisting murine melanoma. Biochim Biophys Acta 2004;1670:172–80.
[24] Yu KY, Kwon B, Ni J, Zhai Y, Ebner R, Kwon BS, et al. A newly identified member of tumor necrosis factor receptor superfamily (TR6) suppresses LIGHT-mediated apoptosis. J Biol Chem 1999;274:13733–6.
[25] Fearon ER, Itaya T, Hunt B, Vogelstein B, Frost P. Induction in a murine tumor of immunogenic tumor variants by transfection with a foreign gene. Cancer Res 1988;48:2975–80.
[26] Tanaka K, Gorelik E, Watanabe M, Hozumi N, Jay G. Rejection of B16 melanoma induced by expression of a transfected major histocompatibility complex class I gene. Mol Cell Biol 1988;8:1857–61.
[27] Yu P, Fu YX. Targeting tumors with LIGHT to generate metastasis-clearing immunity. Cytokine Growth Factor Rev 2008;19:285–94.
[28] Loeffler M, Le'Negrate G, Krajewska M, Reed JC. Attenuated Salmonella engineered to produce human cytokine LIGHT inhibit tumor growth. Proc Natl Acad Sci U S A 2007;104:12879–83.
[29] Shaikh RB, Santee S, Granger SW, Butrovich K, Cheung T, Kronenberg M, et al. Constitutive expression of LIGHT on T cells leads to lymphocyte activation, inflammation, and tissue destruction. J Immunol 2001;167:6330–7.
[30] Lukashev M, LePage D, Wilson C, Bailly V, Garber E, Lukashin A, et al. Targeting the lymphotoxin-beta receptor with agonist antibodies as a potential cancer therapy. Cancer Res 2006;66:9617–24.